Progress in
Physical Geography

Runoff and sediment dynamics induced by the "Grain for Green" programme: a case study in the Three Gorges Reservoir Area, China

Journal:	*Progress in Physical Geography*
Manuscript ID	PPG-25-029.R1
Manuscript Type:	Research Article
Keywords:	the SWAT+ model, Three Gorges Reservoir Area, the "Grain for Green" programme, runoff and sediment dynamics, climate change

Abstract:	In the context of climate change, large-scale vegetation restoration projects have significantly altered hydrological processes. However, existing studies have primarily focused on the impact of the "Grain for Green" programme (GGP) on hydrological dynamics in arid areas, largely neglecting humid regions. To help close this gap, we simulated streamflow and sediments yield in the Three Gorges Reservoir Area (TGRA), an important ecological zone in China, using the SWAT+ model. We differentiated the effects of the GGP and climate change on streamflow and sediment yield in different hydrological periods. The results show that sediment yield responds more intensely to variations in vegetation composition compared to water yield. From 2000 to 2020, reforestation has significantly reduced annual sediment yield by an average of 802.6 kg/ha. Climate change was identified as the main driver of the changes in runoff and sediment yield. Furthermore, the effects of reforestation exhibit seasonality, with runoff increasing during the dry season and sediment yield decreasing during the flood season. The GGP also reduces runoff and sediment yield extremes and promotes the stability of the water-sediment relationship. In addition, projections of future climate scenarios from 2025 to 2050 indicate an upward trend in total runoff and a downward trend in soil retention. This study provides insights into the impacts of the GGP and climate change on hydrological processes in humid regions and offers guidance for future development pathways.

Runoff and sediment dynamics induced by the "Grain for Green" programme: a case study in the Three Gorges Reservoir Area, China

Abstract: In the context of climate change, large-scale vegetation restoration projects have significantly altered hydrological processes. However, existing studies have primarily focused on the impact of the "Grain for Green" programme (GGP) on hydrological dynamics in arid areas, largely neglecting humid regions. To help close this gap, we simulated streamflow and sediments yield in the Three Gorges Reservoir Area (TGRA), an important ecological zone in China, using the SWAT+ model. We differentiated the effects of the GGP and climate change on streamflow and sediment yield in different hydrological periods. The results show that sediment yield responds more intensely to variations in vegetation composition compared to water yield. From 2000 to 2020, reforestation has significantly reduced annual sediment yield by an average of 802.6 kg/ha. Climate change was identified as the main driver of the changes in runoff and sediment yield. Furthermore, the effects of reforestation exhibit seasonality, with runoff increasing during the dry season and sediment yield decreasing during the flood season. The GGP also reduces runoff and sediment yield extremes and promotes the stability of the water-sediment relationship. In addition, projections of future climate scenarios from 2025 to 2050 indicate an upward trend in total runoff and a downward trend in soil retention. This study provides insights into the impacts of the GGP and climate change on hydrological processes in humid regions and offers guidance for future development pathways.

Keywords: the SWAT+ model, Three Gorges Reservoir Area, the "Grain for Green" programme, runoff, sediment yield

1. Introduction

Large-scale vegetation restoration measures are increasingly being implemented worldwide to mitigate global warming and extreme weather events (Lewis et al., 2019; Cai et al., 2020). In China, extensive "grain-for-green" and grazing exclusion practices have been implemented over the past 20 years (Wu et al., 2023). Specifically, the "Grain for Green" programme (GGP) was carried out in two phases, i.e., from 1999 to 2013 and from 2014 to 2019 (NFGA, 2020). The program aimed to prevent soil erosion, mitigate flooding, store carbon, and improve livelihoods by increasing forest and grassland cover on cultivated slopes and converting cropland, barren hills, and wasteland to forests (Bryan et al., 2018). Under such large-scale vegetation restoration measures, hydrological processes experience significant changes. For example, the GGP has been confirmed to increase precipitation and reduce sediment yield in China's Loess Plateau (Bai et al., 2024; Jian et al., 2015). Therefore, planning for future changes under these ecological restoration policies requires a comprehensive understanding of possible hydrological effects.

At the watershed scale, hydrological research is primarily concerned with the effects of vegetation changes on hydrological processes such as runoff generation and sediment transport (Wang et al., 2021). Numerous studies have addressed the effects of vegetation restoration measures on hydrological processes (such as precipitation, soil

moisture and evapotranspiration), particularly in arid and semi-arid regions such as China's Loess Plateau (Bai et al., 2024; Zhou et al., 2024a). However, most previous studies were limited to arid and semi-arid regions, and comprehensive assessments of the hydrological impacts of the GGP in humid areas such as the Yangtze River Basin remain relatively scarce. The Three Gorges Reservoir Area (TGRA) serves as an important ecological barrier zone in the Yangtze River Basin. Located upstream of the Three Gorges Dam, it has crucial influences on the ecological conditions and hydrological stability necessary for the reservoir's normal operation. With its unique ecological location and function, the TGRA is a suitable study area.

In the past two decades, dam construction and ecological policies have considerably altered the landscape pattern in the TGRA. Wang et al. (2019) found that reforestation reduced total runoff and total phosphorus delivery in certain sub-watersheds in the TGRA, revealing the spatial effects of reforestation. Soil erosion is commonly triggered by precipitation events, has also been highlighted in the Yangtze River basin because reduced sediment yield is vital for ensuring the operation of the Three Gorges Dam (Li and Wang, 2024; Zhou et al., 2009). Xu et al. (2020) evaluated the effect of three major ecological programs on ecological rehabilitation in the TGRA, and concluded that the GGP effectively controlled soil erosion over an area of 2196 km^2. Although previous studies have provided basic knowledge of the hydrological impacts of the GGP in the TGRA, systematic analysis of seasonal variations remains limited. Driven by climate factors (Hattermann et al., 2015; Hagemann et al., 2013) and human activities (McFarlane et al., 2012), hydrological processes exhibit distinct

seasonal characteristics. Thus, assessing the seasonal effects of reforestation policies on key hydrological processes in the TGRA is necessary, but only few studies have assessed the seasonal effects of the GGP in the TGRA thus far.

Many studies have examined hydrological responses to climate or land use change using observation data (Yifru et al., 2021; Daneshi et al., 2021) and hydrological model simulations (Derepasko et al., 2023; Liu et al., 2010). Specifically, hydrological responses have been quantified using distributed hydrological models, such as the SWAT model (Arnold et al., 2012), VIC model (Liang et al., 1996), HSPF model (Duda et al., 2012), and SWMM model (Lowe, 2010). In particular, SWAT+, the updated version of SWAT (Bieger et al., 2017), features enhanced capacity for addressing the specific complexities of the TGRA. As the watershed outlet of the upper Yangtze River, the TGRA exhibits a steep, heterogeneous terrain and has undergone significant conversion of sloping cropland to forest. The advanced spatial discretization of landscape units to hydrologic response units in SWAT+ uniquely captures these topographic variations and land-use transitions. Meanwhile, its refined algorithms for land management scheduling are critical for simulating the influences of reforestation (Wallington and Cai, 2023). Furthermore, the various global implementations of SWAT+ (Nkwasa et al., 2020; Leone et al., 2024; Castellanos-Osorio et al., 2023) have proven the flexibility and effectiveness of the model in simulating hydrology-related processes under changing environmental conditions (Bieger et al., 2017).

This study quantified the responses of hydrological processes and sediment yield to reforestation and climate change in the TGRA using the SWAT+ model. The primary

objectives were to: (1) simulate water yield and sediment yield in the TGRA over the past 20 years; (2) assess the effects of reforestation and climate change on water yield and sediment yield during different hydrological periods; and (3) predict future changes in water yield and soil retention under different climate scenarios and land-use development patterns. These findings will provide a basis for assessing the hydrological impact of reforestation measures and policies in humid regions, further improving environmental protection and addressing future climate change risks.

2. Materials and methods

2.1. Study area and research framework

Located between 28°28’ – 31°44’N and 105°49’ – 111°39’E (Fig. 1), the TGRA lies at the intersection of Hubei province and Chongqing city in China and extends along the main stream of the Yangtze River. In this study, the land surface from the Zhutuo section of the main stream of the Yangtze River to the Three Gorges Dam was taken as the study area, covering approximately 64, 000 km^2 (Chen et al., 2019). Under the submergence induced by the Three Gorges Dam and the implementation of reforestation policies, land-use patterns in the TGRA have changed significantly. From 2000 to 2013, the area of reforestation in the upstream regions, including the TGRA, covered 13990 km^2 (NFGA, 2020). From 2014 to 2019, the area of reforestation in the TGRA and upstream of Hubei and Chongqing covered approximately 4352 km^2 (NFGA, 2020). In the implementation of shelterbelt construction projects in the TGRA, the highest priority is to protect water and soil conservation banks. The construction area

covers about 47 counties in Hubei province and Chongqing city (https://www.forestry.gov.cn/main/4862/20201209/114128738802192.html). A protection system comprising reservoir, soil and water conservation, as well as sand and silt control has been established along the bank and mountain system of the reservoir, with the main stream of the Yangtze River serving as the primary axis.

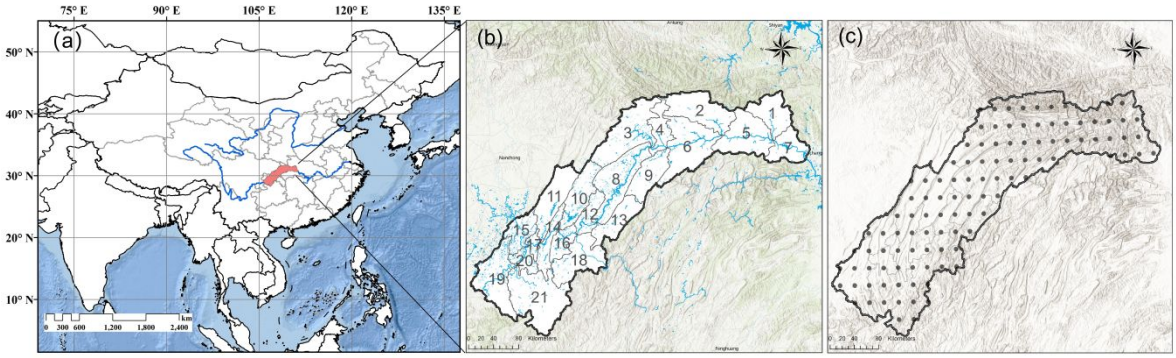

Fig. 1. (a) Geographical location of the TGRA, (b) subbasins of the TGRA, and (c) point stations of CN05.1.

The research framework consists of four parts (Fig. 2). Firstly, we selected water yield and sediment yield indicators for the SWAT+ model simulations. There two hydrological processes were selected considering their direct interactions with climate change and vegetation composition. Secondly, to quantify the impacts of reforestation and climate change during different hydrological periods, we designed various scenarios for comparison and analysis. Here we define June, July, August, and September as the flood season, December, January, February, and March as the dry season, and the other months as the normal season. In addition, the impacts of the GGP on streamflow and sediment extremes were also explored. Third, to acknowledge strategies for adjusting land development in the face of future climate, we modeled three land-use development patterns using the Patch-generating Land Use Simulation

(PLUS) model, and simulated future water yield and sediment retention under two Shared Socioeconomic Pathways (SSP245 and SSP585). Finally, by analyzing the simulation results and comparing with other research, we reveal and discuss the effect mechanism of the GGP and climate change.

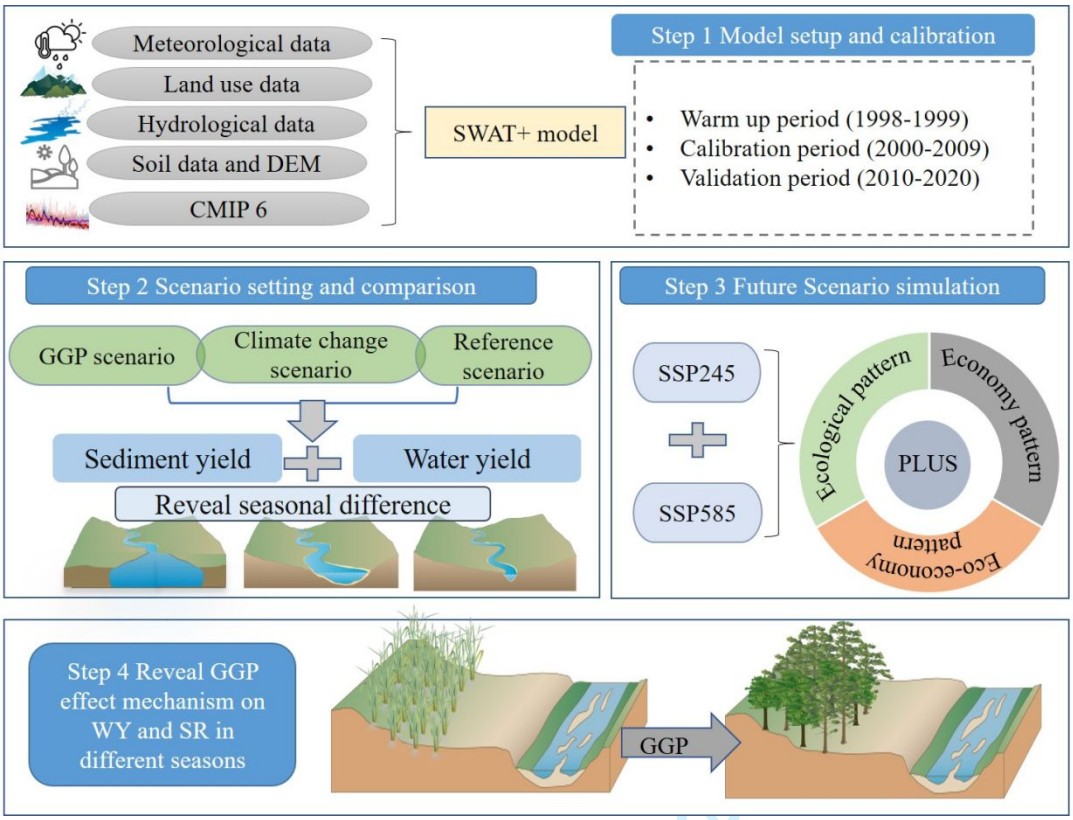

Fig. 2. Research framework (some illustrations are downloaded from https://ian.umces.edu/media-library/). Note: WY is water yield, and SR is soil retention.

2.2. Data

The SWAT+ model was driven and validated using meteorological data, topographic data, land use/cover data, soil data, and hydrological observations (Table 1). Meteorological data were obtained from the CN05.1 gridded dataset (Wu and Gao, 2013), which provides daily precipitation, maximum and minimum temperature, sunshine hours, wind speed, and relative humidity at a spatial resolution of 0.25°. To

better reflect the spatial heterogeneity of the climate in the TGRA, we selected data covering the period 1961–2020 from 108 grid points of the CN05.1 dataset that overlap with the TGRA. In addition, daily climate projections (precipitation and temperature) from three CMIP6 models were used for future scenario analysis. The projection data were downloaded from the ESGF data portal (https://esgf-node.llnl.gov/) and covers the period from 2000 to 2050. Land use/cover data for the years 2000, 2010, and 2020 with a spatial resolution of 1 km were obtained from the Resource and Environment Science and Data Center of China (http://www.resdc.cn). To ensure matching with the SWAT+ model land use database, the original land use classes were reclassified into 7 types, namely cultivated land, forests, grassland, shrubland, waterbody, built-up land, and unused land. Soil data with a spatial resolution of 1 km were retrieved from the Harmonized World Soil Database. DEM data with a 30 m spatial resolution were used to delineate watershed boundaries, define stream networks, and derive slope and elevation information. The SWAT+ model was calibrated and validated using streamflow and sediment data. Monthly observations of streamflow from 2000 to 2020 were collected from four hydrological stations in the TGRA, namely Yichang, Beibei, Cuntan, and Wanxian. However, sediment yield data were available only for Yichang station from 2006 to 2020. These data were collected from the Yangtze River Water Resources Commission and Qin et al. (2020).

Additionally, remote sensing-based vegetation indicators were used for analyzing vegetation dynamics. Monthly Leaf Area Index (LAI) data covering the period 2000–2020 were obtained from the GLASS LAI MODIS dataset at a resolution of 0.05°,

while Normalized Difference Vegetation Index (NDVI) data for the same period were derived from a 250 m resolution dataset compiled by Gao Jixi (2024).

Table 1 Primary data used in this study

Data Type	Source	Use	Resolution
Daily precipitation, average /maximum/minimum temperature, sunshine hours, average wind speed, and relative humidity from 1961 to 2020	CN05.1 dataset (Wu and Gao, 2013)	Input data of the SWAT+ model. CN05.1 data from 1961 to 2014 was used as the evaluation data of GCMs.	0.25°
Soil data	The Harmonized World Soil Database		1 km
Land use/cover data in 2000, 2010 and 2020	http://www.resdc.cn		1 km
DEM data	http://www.resdc.cn		30 m
Daily precipitation, maximum/minimum temperature of CNRM-CM6-1, NorESM2-LM, and INM_CM5_0 model from 2000 to 2050	https://esgf-node.llnl.gov/search/cmip6/		0.25°
Monthly observed streamflow data from 2000 to 2020 of Yichang, Beibei, Cuntan and Wanxian hydrological stations. Monthly observed sediment yield data of Yichang station from 2006 to 2020	The Yangtze River Water Resources Commission and Qin et al. (2020)	Model calibration data	m^3 /s, tons
Monthly LAI data from 2000 to 2020	GLASS LAI MODIS data set	Change analysis of ecohydrological elements	0.05°
NDVI from 2000 to 2020	Gao Jixi (2024)		250 m

2.3. SWAT+ model

2.3.1 Model description

The SWAT model is a physically-based, semi-distributed hydrological model developed to quantify the effects of land management practices in large, complex watersheds with diverse soils, land use, and management conditions over long periods (Arnold et al., 2012). With these advantages, the model has been used in many studies to assess hydrological processes (Janjić and Tadić, 2023; Brighenti et al., 2019; Shi et al., 2011; Xiong et al., 2019; Francesconi et al., 2016; Uniyal et al., 2023). SWAT+ is an updated version of SWAT that is based on the same equations but offers greater flexibility in the configuration of model processes (Bieger et al., 2017; Noori and Kalin, 2016). Regarding the model setup, we used the new open-source QGIS interface for

SWAT+. This interface is based on the concept of hydrologic response units (HRUs) and landscape units (LSUs) as smaller-scale subdivisions of the sub-basins, to separate upland and floodplain processes are separated (Bieger et al., 2017). In SWAT+, the different elements of a watershed, e.g., LSUs, HRUs, aquifers, ponds and reservoirs, inlets, point sources, and channels, are defined as spatial objects. The user can define hydrologic interactions between different spatial objects to represent the physical characteristics of a watershed as realistically as possible (Bieger et al., 2019).

2.3.2 Water yield and soil conservation calculation

The SWAT+ model defines total water provisioning supply as the water that leaves sub-basins and flows into a river within a time step (Arnold et al., 2012). The water balance equation used in the SWAT+ model is as follows (Noori and Kalin, 2016):

$$SW_t = SW_o + \sum_{i=1}^{t} (R_{day} - Q_{surf} - E_\alpha - W_{seep} - Q_{gw}) \quad (1)$$

where SW_t and SW_O are the final and initial water contents (mm), t is the time (days), R_{day} is the amount of precipitation on day i. Q_{surf} is the surface runoff on day i (mm), E_α is the amount of evapotranspiration on day i (mm), W_{seep} is the amount of percolation and bypass flow exiting the soil profile bottom on day i (mm), and Q_{gw} is the amount of return flow on day i (mm).

We estimated the supply of soil under conservation measures based on the modified universal soil loss equation in the sediment erosion section of the SWAT+ model (Zhou et al., 2024b; Wang et al., 2022). The C_{usle} and P_{usle} factors of the formula were set to 1, which represents the condition of bare soil without any vegetation or conservation

measures (Zhou et al., 2024b; Wang et al., 2022). This adjustment allows the estimation of potential soil erosion (SED_p) in the absence of protective factors. On this basis, the amount of soil conserved through ecological protection and land use practices can be quantified by comparing this SED_p with the actual soil erosion (SED_a) under existing land use and management. In this study, sediment yield and soil conservation under past scenarios were estimated and future predictions were made. The formula for the calculation formula is as follows:

$$SC = SED_p - SED_a = 11.8 \times \left(Q_{surf} \times q_{peak} \times area_{hru}\right)^{0.56} \times K_{usle} \times LS_{usle} \times CFRG(1 - C_{usle} \times P_{usle}) \quad (2)$$

where SC, SED_p, and SED_a refer to soil conservation (t), potential soil erosion (t), and actual soil erosion (t), respectively. Q_{surf}, q_{peak} and $area_{hru}$ are surface runoff (mm/ha), peak runoff rate (m^3/s), and HRU area (ha), respectively. K_{usle} is the soil erodibility factor; C_{usle} is the vegetation and management factor; P_{usle} is the factor of soil and water conservation measures; LS_{usle} is the slope length and slope gradient factor; and $CFRG$ is the roughness coefficient.

2.3.3 Model setup and calibration

Based on the imported stream network data downloaded from OpenStreetMap and DEM data, the TGRA was divided into 21 LSUs and 524 HRUs in the QGIS interface. As this study focused on the regional scale assessment of the impact of land use change on water yield and sediment yield, the watershed was not divided into a large number of small watersheds, and this approach can be considered reasonable because the

simulation accuracy was high. In the SWAT+ editor, the spin-up period was set as 1998–1999, the hydrological calibration period as 2000–2010, and the validation period as 2010–2020. As sediment data before 2006 were lacking, the sediment calibration period was set as 2006–2012 and the validation period was 2013–2020. The simulation results of the SWAT+ model were calibrated and evaluated using the SWAT+ Toolbox (https://celray.github.io/SWATPlusToolbox/). The Calibration and Sensitivity Iterative (CALSI) algorithm is a tool in the SWAT+ Toolbox designed for model parameter calibration and sensitivity analysis. CALSI combines parameter optimization and sensitivity analysis to improve model accuracy and ensure reasonable parameter settings. In this study, the goodness of fit of the SWAT+ model was evaluated using the Nash-Sutcliffe efficiency (NS), coefficient of determination (R^2), and percentage bias (PBIAS). The formula of NS, R^2, and PBIAS are as follows (Nash and Sutcliffe, 1970; Xu et al., 2011):

$$NS = 1 - \frac{\sum_{i=1}^{n} (Q_m - Q_s)_i^2}{\sum_{i=1}^{n} (Q_{m,i} - \overline{Q}_m)^2} \quad (3)$$

$$R^2 = 1 - \frac{\left[\sum_{i=1}^{n} (Q_{m,i} - \overline{Q}_m)\,(Q_{s,i} - \overline{Q}_s)\right]^2}{\sum_{i=1}^{n} (Q_{m,i} - \overline{Q}_m)^2 \sum_{i=1}^{n} (Q_{s,i} - \overline{Q}_s)^2} \quad (4)$$

$$PBIAS = 100\% \times \frac{\sum_{i=1}^{n} (Q_m - Q_s)_i}{\sum_{i=1}^{n} Q_{m,i}} \quad (5)$$

where Q_m is the measured volume (the unit of outflow is m^3/s and the unit of sediment yield is tons), Q_s is the simulated volume, and i and n represent the sample number and total sample size, respectively.

2.4. Quantifying relationships of runoff and sediment yield extremes

Referencing Yin et al. (2023), extreme streamflow and extreme sediment yield were defined as values exceeding the 95th percentile during a year to reflect extremely high streamflow or sediment yield characteristics. On this basis, we calculated the sediment rating curve to reveal the variation in extreme runoff and sediment relationships after the implementation of the GGP. We characterized relationships between extreme runoff and sediment according to power-law sediment rating curves, which can be expressed as follows (Gao et al., 2024):

$$S = C_s Q = aQ^{b+1} \quad (6)$$

where, S is the daily sediment yield (t), C_s is the daily sediment concentration (kg/m^3), Q is the daily streamflow (m^3), and a and b are the sediment rating coefficient and exponent (dimensionless), respectively. a represents an index of erosion severity. High values of a indicate intensively weathered materials, which can easily be transported. The exponent b represents the river's erosive power, with large values indicating a strong increase in erosive power even with a small increase in discharge.

2.5. Projected climate change scenarios

The Coupled Model Intercomparison Project (CMIP) provides shared climate simulation data covering the next 50 to 100 years as a foundation for global climate research (Cook et al., 2020). We selected 14 global climate models (GCMs) from the CMIP6 dataset that displayed (Table S2). These models were selected because their good simulation performance for the Yangtze River Basin has been confirmed (Zhu et

al., 2021; Thrasher et al., 2022). Two emission scenarios, SSP245 (+4.5 W/m2; medium forcing middle-of-the-road pathway) and SSP585 (+8.5 W/m2; high-end forcing pathway) (Cook et al., 2020), were selected to represent medium and high-end radiative forcing pathways, respectively.

To address the inconsistent spatial resolutions of CMIP6 GCM outputs, we adopted a statistical downscaling approach based on the CN05.1 gridded observation dataset. The statistical downscaling procedure involved two steps: (1) bias correction through probability density function matching between GCM simulations and CN05.1 observational data over the historical period; and (2) spatial interpolation via bilinear methods. In this manner, systematic errors can be reduced while preserving climate trends projected by the original GCMs. Given that the CMIP6 historical simulations end in 2014 data of and scenarios begin in 2015, the evaluation period was set as 1961–2014 and the future projection period as 2025–2050.

To evaluate the performance of the downscaled GCMs, the performance of different GCMs was evaluated on the basis of the spatial correlation coefficient (R), root mean square error (RMSE), and ratio of spatial standard deviations (Taylor, 2001). As shown in Fig. S4, most GCMs exhibited strong agreement with observations for temperature variables, with R exceeding 0.95 and RMSE values below 2%. In contrast, precipitation showed greater inter-model variability, with RMSE values ranging from 4% to 6%. Therefore, based on the results of comparison result with CN05.1, CNRM-CM6-1, NorESM2-LM, and INM_CM5_0 were selected as the best performing models to serve as climate input data for SWAT+ from 2025 to 2050.

2.6. Projected land use patterns

To explore the long-term impacts of land use change on hydrological processes in the TGRA, we developed three future land use scenarios based on regional policy directions and previous studies (Huang et al., 2022). The simulation process is described in further details in the Supplementary Information. In recent years, the TGRA has received major ecological restoration efforts, such as large-scale reforestation and the Three Gorges Project. Meanwhile, urban expansion has significantly altered the landscape of this area. Considering the need for balancing environmental sustainability and socioeconomic growth, three contrasting development scenarios were constructed to represent potential future trajectories (2025–2050). The ecological scenario emphasizes environmental protection and landscape optimization, prioritizing forest coverage while controlling urban expansion. It aims to optimize landscape patterns by adjusting the proportions of various landscape types. The economic scenario focuses on urban development, but the expansion of construction land is moderated to half the rate observed during the period from 2000 to 2020. The eco-economic scenario integrates both ecological and economic considerations, aiming for a compromise that supports both conservation goals and development needs. The land transition matrices under the three scenarios were set by following the prediction made by Huang et al. (2022) in the TGRA (Table S1). These scenarios provide a framework for assessing the potential effects of policy-driven land use decisions on water yield and sediment retention in the TGRA under changing conditions. Future land use scenarios were simulated using the PLUS model (Liang et al., 2021), and the

simulation results (Fig. S2) were input to the SWAT+ model. To ensure simulation accuracy, we simulated the land use in 2020 and compared the simulation results with the actual land use data of 2020 (Fig. S3). The comparison yielded an overall kappa coefficient of 0.77, which meets the accuracy requirements.

2.7. Scenario design

In the TGRA, reforestation was implemented on sloped cropland with a gradient greater than 15°. Therefore, areas with sloped cropland above 15° that were converted to forest and grassland during 2000–2020 were identified as reforestation zones using ArcGIS. We designed four scenarios to analyze the impact of reforestation and climate change from 2000 to 2020 (Table 2).

- S1: a reference scenario without changes in land use and climate. Data of land use in 2000 and climate from 1990 to 2000 were used as input to the SWAT+ Editor.
- S2: except for reforestation zones, other land use types remain unchanged with reference to 2000. An updated land use dataset with reforestation zones and climate data from 1990 to 2000 was input to the SWAT+ Editor.
- S3: land use in 2020 and climate data from 1990 to 2020 were used as input to the SWAT+ Editor, reflecting both land use change and climate change.
- S4: land use in 2000 and climate data from 2000 to 2020 were used as input to the SWAT+ Editor.

The impact of the reforestation policy can be quantified subtracting S1 from S2 (S2-S1). The total effect of land use changes can be quantified by subtracting S1 from

S3 (S3-S1). The effect of climate can be quantified by subtracting S1 from S4 (S4-S1).

The future scenarios were simulated in a pairwise manner combining by setting three land use development patterns and two climate change scenarios:

- F1, F3, and F5: simulation results of land use under three scenarios and SSP245 were set as input data for the SWAT+ Editor.
- F2, F4, and F6: simulation results of land use under three scenarios and SSP585 were set as input data for the SWAT+ Editor.

Table 2 Scenarios designed in this study

Scenarios	Land use data	Climate data
S1	2000	1990–2000
S2	Other land types of 2000 combined with the reforestation zones	1990–2000
S3	2020	1990–2000
S4	2000	2000–2020
F1	Ecological pattern	SSP245
F2	Ecological pattern	SSP585
F3	Economy pattern	SSP245
F4	Economy pattern	SSP585
F5	Eco-economy pattern	SSP245
F6	Eco-economy pattern	SSP585

3. Results

3.1. Hydrological Calibration

We simulated water yield and sediment yield using the SWAT+ editor and the tool showed good performance after calibration. We conducted a global sensitivity analysis using the Latin Hypercube Sampling (LHS) combined with the One-Factor-at-a-Time (OAT) method embedded in the SWAT+ Toolbox. Ten key parameters related to hydrological and sediment processes were evaluated, including those controlling runoff generation, soil moisture dynamics, and erosion potential (Table 3). The most sensitive parameters were found to be ALPHA, CANMX, USLE_P, and AWC, with sensitivity

indices of 0.28, 0.18, 0.17, and 0.16, respectively. In particular, we calibrated four parameters, CANMX, ESCO, USLE_P, and USLE_K, after which NS result increased by 0.02 to 0.10 and PBIAS decreased by 10 to 20 (Table S3). CANMX, representing the maximum canopy water storage, was calibrated within a range of 0–20 mm to account for the interception effect of vegetation on runoff (Li et al., 2021). ESCO, the soil evaporation compensation factor, was adjusted between 0.2 and 0.5 to reflect soil evaporation dynamics under varying soil moisture conditions. USLE_P, the support practice factor, was set to 0.7 to represent the average level of soil conservation measures in the region, while USLE_K, the soil erodibility factor, was set to 0.4 to capture the typical erodibility characteristics of soils. The parameter calibration afforded satisfactory model performance in simulating both water yield and sediment yield.

Table 3 Sensitivity analysis results of hydrological and sediment-related parameters used in the SWAT+ Toolbox

Parameters	Abs_min	Abs_max	Group	Sensitivity
ALPHA	0	1	aqu	0.28
CANMX	0	100	hru	0.18
USLE_P	0	1	hru	0.17
AWC	0	1	sol	0.16
SOL_k	0	1	sol	0.11
CN2	35	95	hru	0.10
USLE_k	0	0.65	sol	0.09
SURLAG	0.05	24	bsn	0.05
REVAPMN	0	50	aqu	0.05
CHN	-0.01	0.3	rte	0.02

After the calibration and validation of the model for monthly streamflow with several simulations, the SWAT+ exhibited an R^2 range of 0.92–0.94 for the four hydrological stations during the calibration period. The NS coefficient ranged between 0.8 and 0.89, and the absolute PBIAS value ranged from 3.01 to 16.4 (Table 4 and Fig. S5). With NSE, R^2 values greater than 0.8 and the absolute value of PBIAS less than

10, the calibration model results can be considered "very good". Although the values of R^2, NS, and PBIAS were lower in the validation period than in the calibration period, the results can be considered "good" based on the assessment criteria of Chen et al. (2022). The simulation results for monthly sediment yield were not as good as those for streamflow, but they can still be considered satisfactory because they showed R^2 values of 0.57 and 0.54, and NS values of 0.54 and 0.44 in the calibration and validation periods, respectively. As shown in Fig. S6, the simulated sediment yield is consistent with the measured sediment yield for low peaks, but the peak sediment yield could not be captured. This can be explained by the model not considering flood-plain erosion during peak flow conditions when simulating sediment yields (Nepal et al., 2023). Compared with SWAT, SWAT+ offers significantly higher accuracy, for simulating runoff, with there are higher R^2 and NS, and lower absolute PBIAS values, as shown in Fig. S5, S6, and Table S4. Nevertheless, the simulation results remain comparable for sediment yield. Therefore, SWAT+ was selected for all subsequent analyses in this study.

Table 4 Validation and calibration results of simulated runoff

Period	Station	R^2	NS	|PBIAS|
Calibration	Yichang	0.94	0.84	12.02
	Beibei	0.92	0.89	3.01
	Cuntan	0.94	0.82	16.4
	Wanxian	0.93	0.80	16.4
Validation	Yichang	0.87	0.67	12.1
	Beibei	0.92	0.88	0.89
	Cuntan	0.93	0.74	9.75
	Wanxian	0.89	0.74	15.27

3.2. Spatio-temporal dynamics of streamflow and sediments in the TGRA

Before conducting the simulations under the different scenarios, we analyzed the spatio-temporal dynamics of streamflow and sediment yield in the TGRA for the period

2000–2020. The sediment and water yields exhibited more significant variations on an intra-annual scale, with higher values predominantly concentrated in July, August, and September (Fig. 3a). On average, streamflow increased by 2959 million m³/y, 1426 million m³/y, and 239 million m³/y during the flood, normal, and dry seasons (Fig. 3b). Moreover, sediment yield tended to increase particularly especially during the flood season, with an average of 1.77 million tons per year.

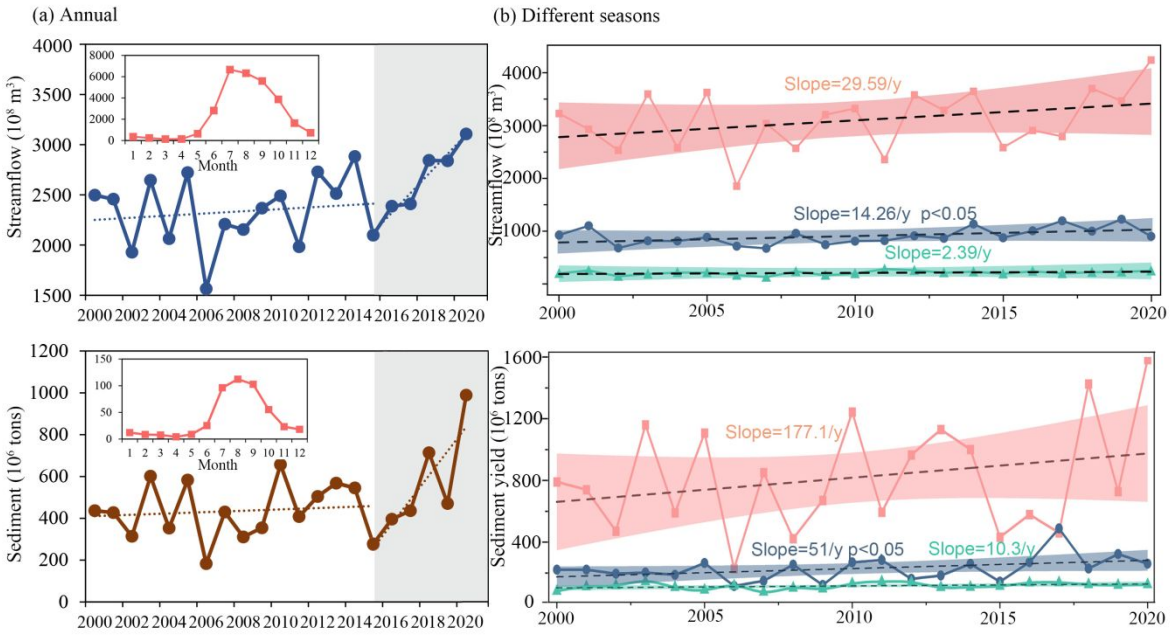

Fig. 3. Temporal changes of (a) annual streamflow and sediment yield, (b) streamflow and sediment yield in different seasons from 2000 to 2020. Pink represents the flood season, blue represents the normal season and green represents the dry season.

To visualize spatial differences in hydrological components, we selected annual average water yield and sediment yield during different hydrological periods (Fig. 4). The most pronounced seasonal difference were observed in sub-basing along the main stream of the Yangtze River, such as sub-basins 4, 5, 6, 7, and 8. In sub-basins far away from the main stream, the differences in water yield and sediment yield were not pronounced between the flood and dry seasons, with water yield around 1000 m³/s and

sediment yield below 10 million tons. In addition, the spatial distribution of water yield and sediment yield showed a trend of gradually increase from the west to the east of the TGRA.

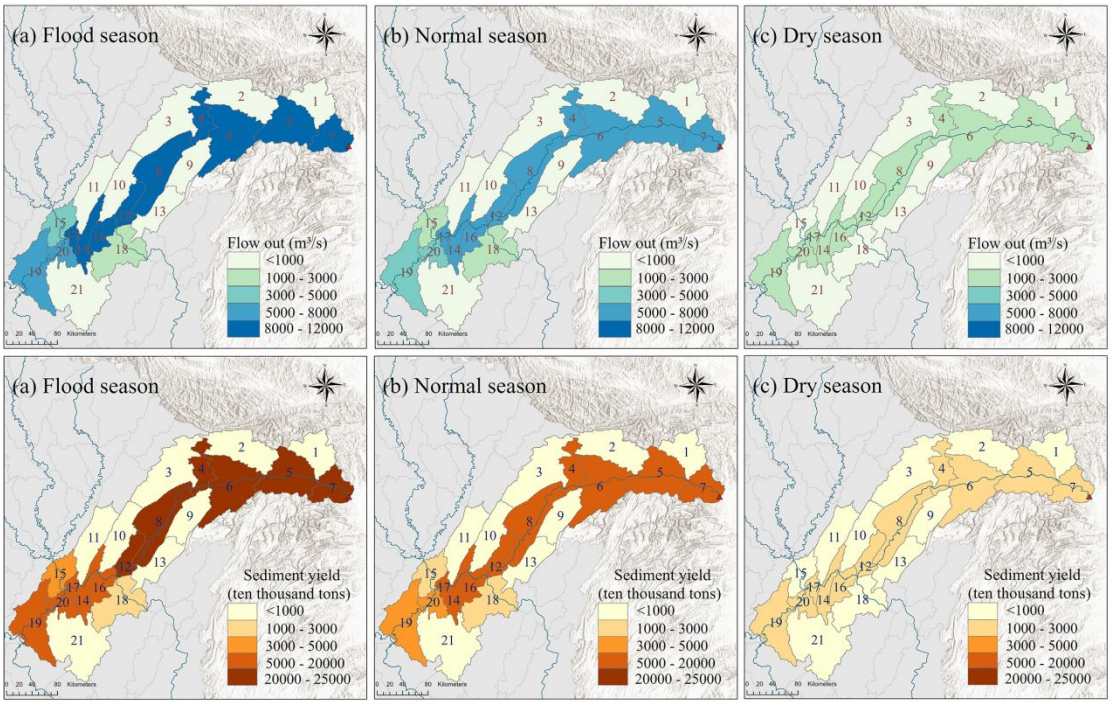

Fig. 4. Annual average water yield and sediment yield during different seasons.

3.3. Impacts of GGP and climate change on water and sediment yield

3.3.1 Water and sediment yield variations among vegetation types

We analyzed cropland, forest, grassland, and shrubland to compare streamflow and sediment yield among different vegetation types. As shown in Fig. 5, variations in streamflow and sediment yield exhibit seasonal differences, with the largest most variation during the flood season and minimal variation differences in the dry season. Forests were the largest contribute to water yield in the dry season, while grasslands and shrublands dominated during the wet season. Under climate and land-use change scenarios, water yield increased compared to the S1 scenario, with the highest difference of 10 mm. In the reforestation scenario, all vegetation types exhibited

increased water yield compared to the S1 scenario, with forests showing the largest increase at nearly 3 mm. In the normal and dry seasons, climate change induced increases in water yield across all vegetation types. Differences in sediment yield among vegetation types were more pronounced than differences in water yield. In all scenarios, farmland exhibited the highest sediment yield. Under the reforestation scenario, sediment yield from cropland and forest decreased. Similarly, sediment yield decreased under the climate and land use change scenarios as well. Overall, sediment yield showed more significant variations than water yield, highlighting the stronger influence of vegetation composition on sediment dynamics during the flood season.

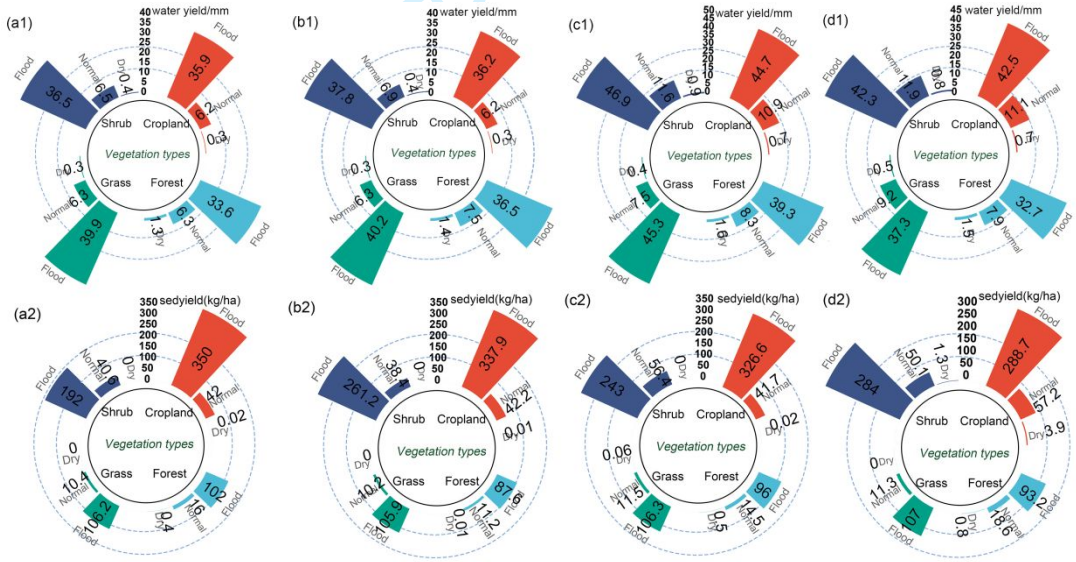

Fig. 5. Annual average water yield (mm) and sediment yield (kg/ha) across of various vegetation types during different seasons. (a) S1, (b) S2, (c) S3, and (d) S4. Number 1 represents the water yield and number 2 represents the sediment yield. The heatmap was plotted through https://www.bioinformatics.com.cn, an online platform for data analysis and visualization

Based on the results obtained under the abovementioned scenarios, we also quantified and assessed the impacts of the GGP and climate change on water and sediment yield (Table 5). The GGP had more pronounced effects on sediment yield than on water yield, reducing annual average sediment yield by 802.6 kg/ha. Although

runoff showed a slight increase, the simulated annual sediment yield decreased because of the reduction of sloped farmland. Increased canopy interception reduces infiltration and may slightly enhance surface runoff, but the improved vegetation cover stabilizes the soil, thereby leading to a substantial reduction in sediment yield (Bunel et al., 2025). In contrast, other land changes such as conversions between built-up and cultivated land increased the sediment yield by 761.2 kg/ha. On the whole, land use change resulted in a reduction of average annual sediment yield by 41.5 kg/ha. Climate change significantly reduced water yield and sediment yield. Under the combined impact of land use changes and climate change, sediment yield and streamflow decreased by 20,024 kg/ha and 5479 m^3/s, respectively, compared to the reference scenario.

Table 5 The influence of different factors on runoff and sediment

Influencing factors	Annual average runoff (m^3/s)	Annual average sediment yield (kg/ha)
GGP	+25	–802.6
Total land use changes	+20,810	–41.5
Other land use changes (deduct GGP effect)	+20,785	+761.2
Climate change	–26,290	–19,982
Climate and land use change	–5479	–20,024

3.3.2 Seasonal difference and impacts on the relationship between extreme runoff and sediment yield

The impacts of different factors on water yield and sediment yield exhibit spatial variations across different sub-basins (Figs. 6 and 7). The GGP had a negative effect on sediment during the flood season and a positive influence on runoff during the dry season. In sub-basin 7, the flow outlet of the TGRA, runoff increased by 28.5 m^3/s. In sub-basins 5 and 7, reforestation primarily reduced sediment yield during the flood and normal seasons. The reduction in sediment yield induced caused by reforestation

intensified from the west to the east. Reforestation had a weaker effect on runoff compared to the total land use change, with the effect concentrated in sub-basins along the main stream of the Yangtze River, particularly in sub-basins 4, 5, 6, 7, and 8. Land use changes increased sediment yield, but the GGP had a stronger influence, leading to an overall reduction in sediment yield. During the flood season, the sediment yield of sub-basins decreased in the eastern TGRA. In contrast, land use changes during the dry season led to an increase in sediment yield, concentrated in the eastern TGRA, with an upward trend from the west to the east. Climate change had a stronger influence on runoff and sediment yield than land use changes, especially during the flood season. Climate change exhibited the strongest negative effect in sub-basins 5, 7, and 16 during the flood season. The reduction in runoff was smaller during the normal and dry seasons. Reductions in sediment yield induced by climate change coincided with the spatial distribution of sediments.

Overall, climate change is the dominant factor affecting runoff and sediment yield, exerting stronger effects than land use changes. It shows negative effects in the eastern TGRA but positive effects in the western. The GGP has more significant seasonal effects on sediment yield than on runoff, mainly reducing sediment yield during the flood and normal seasons, although the effects are weaker smaller than those of total land use changes.

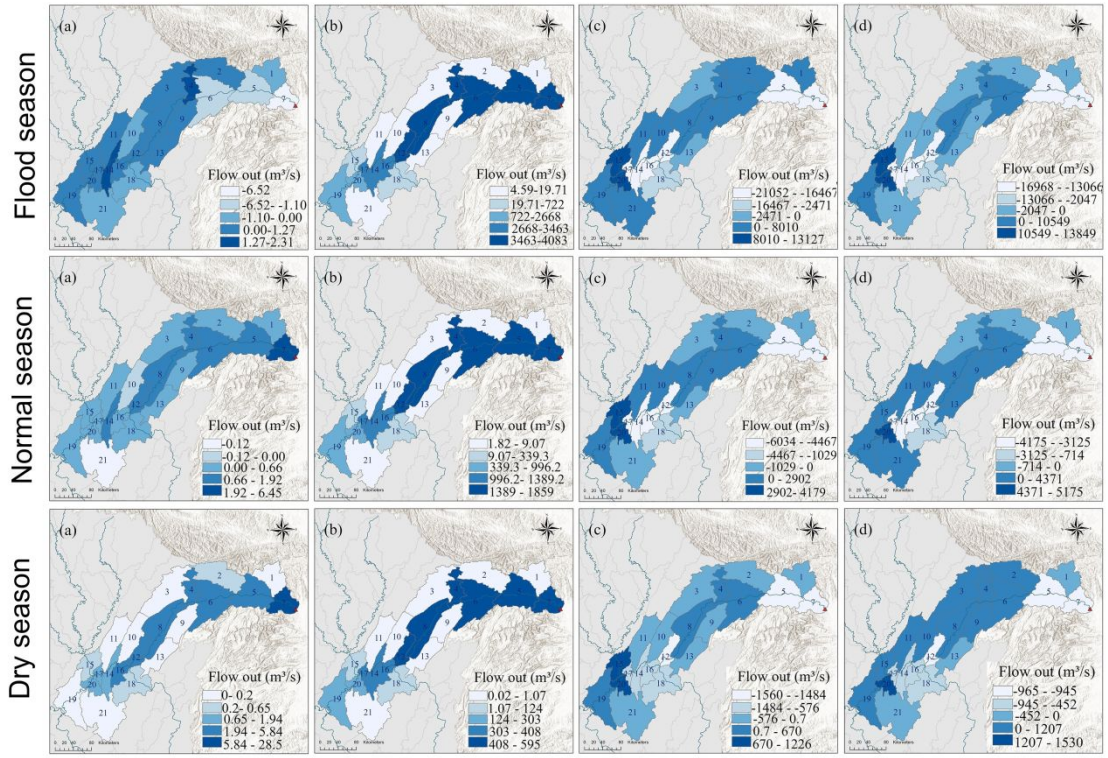

Fig. 6. Influence of different factors on water yield in the flood, normal, and dry seasons. (a) GGP, (b) total land use impacts, (c) climate change (d) total impacts of climate change and land use change

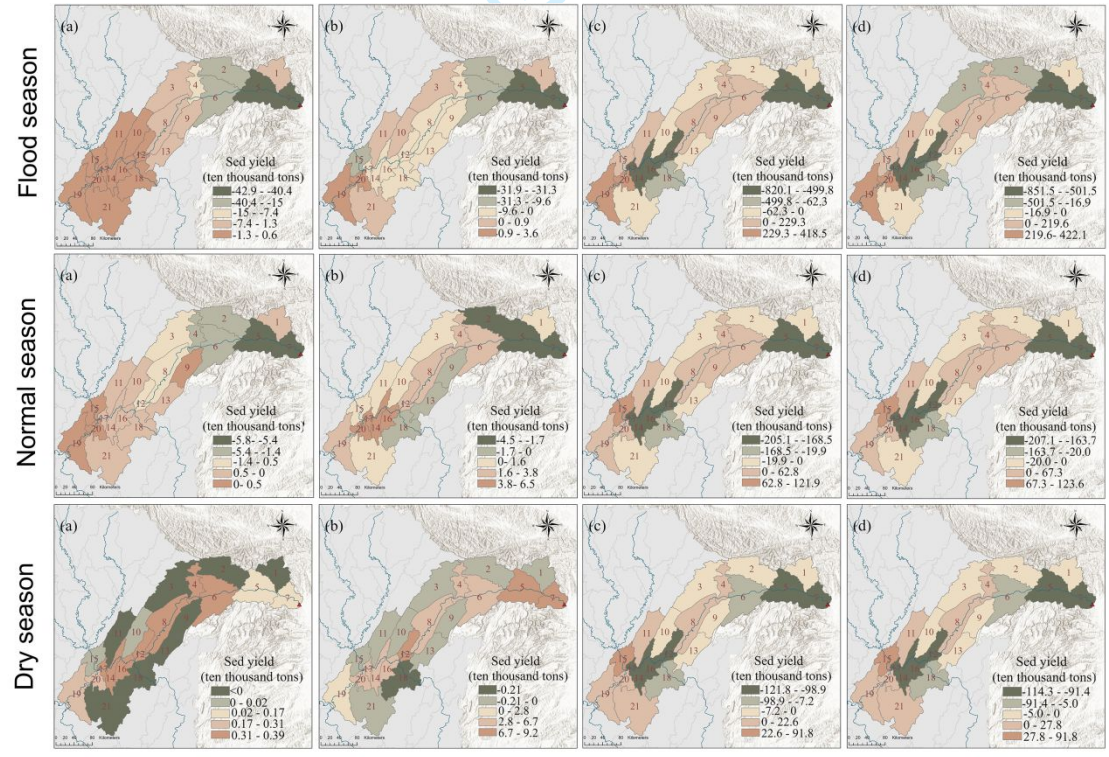

Fig. 7. Influence of different factors on sediment yield in the flood, normal, and dry seasons. The sequence number of graphs is the same as in Fig.6.

To further investigate the impact of the GGP on extreme runoff and sediment yield,

we selected sub-basin 2 for further analysis. This sub-basin features which has the largest area of reforestation, covering 41% of the area. In particular, extreme precipitation was accompanied by extreme sediment yield during the summer months (Fig. 8a and b). Compared to the reforestation scenario, the non-reforestation scenario showed an increase in parameter *a*, from 0.03 to 0.64, and a decrease in parameter *b*, from 3.45 to 2.85, indicating larger soil erodibility and sediment source availability (Yin et al., 2023). This implies a larger amount of sediments and higher susceptibility of soil to erosion. Conversely, under the reforestation scenario, increased vegetation cover will reduce the likelihood of extreme water yield and soil erosion by precipitation, thus supporting more stable water-sediment relationships (Wang et al., 2016). As shown in the box plot in Fig. 8e, runoff and sediment yield extremes definitely showed prominent downward trends under the reforestation scenario. Therefore, reforestation promotes the stability of the water-sediment relationship.

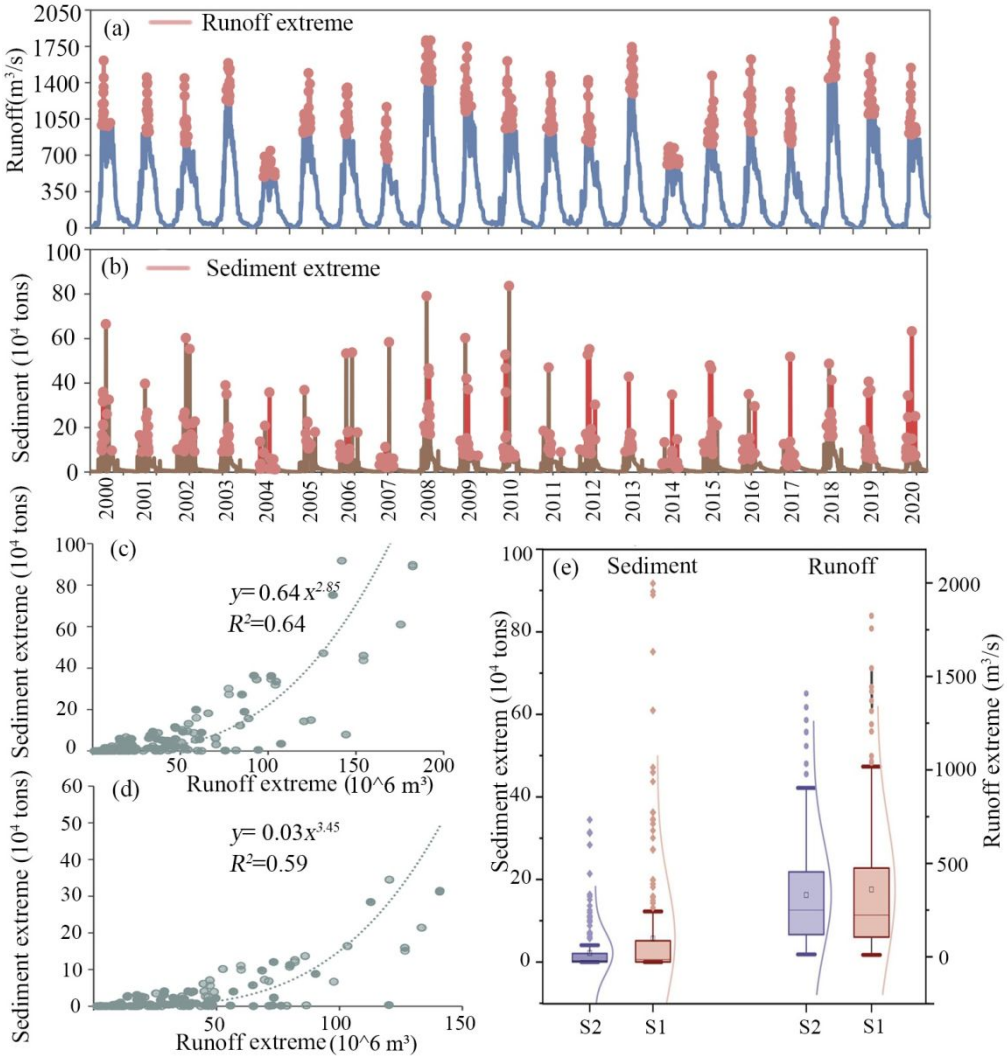

Fig. 8. Impacts of the GGP on extreme streamflow and sediment yield (sub-basin 90 was taken as an example because it has the largest area of land conversion from farmland to forest is the most in this basin). (a) Daily streamflow and extreme streamflow, (b) daily sediment yield and extreme sediment, (c) and (d) the relationships of streamflow and sediment yield extremes of S1 and S2, and (e) box plot of daily streamflow and sediment yield extremes of S1 and S2.

3.4. Projected water yield and soil conservation under future scenarios

We used soil retention and water yield as indicators for future scenarios. The prediction results under future climate scenarios and land-use patterns indicate that water yield and soil retention vary along different directions (Fig. 9). Although water yield and soil retention did not exhibit significant trends, water yield is projected to

increase from 12.96% to 19.3% from 2025 to 2050 compared to the past period (2000–2023). While soil retention is projected to decline from 17.85% to 22.63%. Climate change has a stronger influence on runoff than on land use. Under the changing climate, the variation in runoff under each pattern is minor, with a difference of less than 1%. However, their variations are significant between climate scenarios. The differences in runoff and soil retention between SSP245 and SSP585 are approximately 6% and 4%, respectively. Eekhout and Vente (2020) employed various soil erosion models to simulate the amount of soil erosion in the Mediterranean region under future climate change scenarios. The results, also obtained using the MUSLE soil erosion module in SWAT, also indicated that soil loss would significantly increase in the future.

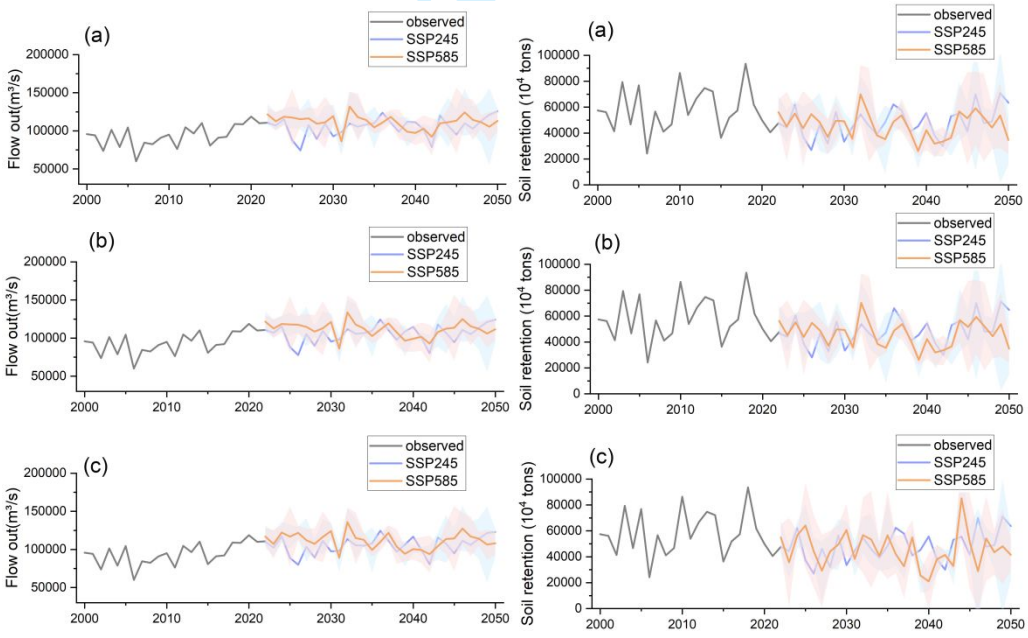

Compared to 2000-2023	SSP245 Water yield	SSP585 Water yield	SSP245 Soil retention	SSP585 Soil retention
(a) Eco	Increase by 12.96%	Increase by 19.17%	Decrease by 18.11%	Decrease by 22.52%
(b) Eco-economy	Increase by 13.08%	Increase by 19.29%	Decrease by 17.85%	Decrease by 22.20%
(c) Economy	Increase by 13.16%	Increase by 19.30%	Decrease by 18.40%	Decrease by 22.63%

Fig. 9. Predictions of water yield and sediment yield under different scenarios. (a) ecological land use pattern, (b) eco-economic use pattern, (c) economic land use pattern. The shades represent one standard deviation among models

4. Discussion

4.1. Effect mechanisms of GGP on runoff and sediment yield

Although many studies literature reports have confirmed that vegetation restoration affects eco-hydrological processes, no consensus has been reached on whether the overall impact is positive or negative (Tianjiao et al., 2023; Wang et al., 2023). In this study, vegetation restoration showed positive effects in the TGRA, in agreement with Xu et al. (2020). In the past twenty years, the area of forests in the TGRA has significantly increased, and the forest coverage rate has reached 58.49% (Fig. 10), leading to significant increases in LAI and NDVI ($p<0.05$). Given that the TGRA has a humid climate, reforestation does not pose the same threat to soil moisture or water resources as it does in arid or semi-arid areas (Sun et al., 2006; Jian et al., 2015). Previous research revealed a significant negative correlation between vegetation changes and water resources, with runoff and runoff coefficients increasing significantly as forests and grasslands are converted to cropland (Wang et al., 2021; Chen et al., 2020). However, in humid and large watersheds with complex topography, vegetation changes have a smaller effect on water yield (Wang et al., 2021). Factors influencing water yield include precipitation, vegetation structure, topography, and evapotranspiration (Rockström et al., 2023; Li et al., 2015). On steep slopes, natural vegetation with complex structures can reduce surface runoff and significantly increase baseflow and low flow volume (Sidle et al., 2017; Molina et al., 2012). In comparison, planted forests have a smaller impact on runoff generation, although baseflow it can

still increase. In the TGRA, reforested land primarily consists of planted forests that were converted from cropland, and their influence on surface runoff is thus relatively small.

Regarding soil retention, reforestation in the TGRA has significantly reduced sediment yield, surpassing the sediment increases associated with other land transformations, such as urban construction. This reflects the positive effect of the GGP on soil retention in the TGRA (Huang et al., 2023). Compared to runoff, vegetation restoration has a more pronounced effect of reducing sediment yield, especially in humid regions. Increased in vegetation cover can weaken raindrop impact during heavy rainfall, thus effectively preventing soil erosion (Bai et al., 2024; Luo et al., 2021). Additionally, vegetation restoration can improve soil aggregate stability, enhance soil physical and chemical properties, and increase soil permeability, which improve soil resistance to erosion (Zhu et al., 2018). Consequently, surface runoff and sediment loss are reduced. In addition, the effects on sediment yield also vary according to the vegetation type. Studies have shown that the complex vertical structure of vegetation, including tree canopies, shrubs, herbaceous layers, litter, and root systems, can directly or indirectly influence runoff and sediment generation by altering hydrological processes and rainfall redistribution patterns (Li et al., 2015). Vegetation with well-developed root systems help improve soil physical properties, enhance soil permeability, and reduce surface runoff. The stabilizing and binding effects of roots play a critical role in soil retention (Sun et al., 2014; Bai et al., 2024; Wang et al., 2019). Furthermore, slope is an important topographic factor affecting soil erosion. Runoff

velocity is higher on steep slopes, increasing the susceptibility of soil to erosion,. Gebre et al. (2024) confirmed that the occurrence of there was widespread soil loss and high sediment yield on cultivated land dominated by moderate, steep, and very steep slopes with little vegetation and barren areas. Therefore, the soil conservation effect of vegetation restoration is more significant on sloping cropland. In the TGRA, the GPP has primarily been implemented in sloping cropland, where steep cropland is transformed into planted forests. Therefore, the comprehensive effects of slope, soil, root system, and vegetation significantly reduces the risk of soil erosion (Zhang et al., 2015; Bai et al., 2024).

Additionally, climate change plays a dominant role in the dynamics of runoff and sediment yield. Over the past few decades, the intensity of the East Asian monsoon has gradually weakened, leading to decreased precipitation and consequently reduced runoff and sediment generation in the TGRA (Zhao et al., 2023). Previous studies have shown that climate change has had a significant impact on runoff and sediment yield in the TGRA (Zhang et al., 2017). Although human activities are also major contributing factors, the declines in water yield and sediment yield in the TGRA are primarily driven by the reduction in precipitation. This is in agreement with Wang and Sun (2021), who reported that although human activities are the primary driver of the decline in actual sediment yield in the Yellow River, changes in precipitation and rising temperatures have also played a determinable role over the past few decades.

4.2. Seasonal characteristics during different hydrological periods

The effects of the reforestation policy in the TGRA on the hydrological processes exhibit significant differences across various hydrological periods, highlighting its seasonal characteristics (Fig. 10). During the flood season, rainfall is the primary driver of runoff, soil erosion, and nutrient loss (Liu et al., 2014). During heavy rainfall, raindrops have a stronger impact on the topsoil, intensifying water and soil erosion. During the flood season, rainfall exhibits a certain correlation with the reduction of runoff and sediment yield. The particularly notable role of reforestation in the TGRA in reducing sediment yield during the flood season can be explained by two main reasons. First, increased rainfall during the flood season leads to greater runoff and sediment flow; second, the interception by forest vegetation on runoff is relatively weaker during the flood season compared to the dry season. Wang et al. (2019) pointed out that the large water volume and high runoff velocity during the flood season limit the effectiveness of vegetation interception. Wang and Sun (2021) also found that the proportion of runoff reduction is smaller than that of sediment transport in the Yellow River Basin. In addition, extreme flood and sedimentation events are more likely to occur during the summer. In this regard, revegetation measures can substantially mitigate the extremes and possible peaks in a power function form, as confirmed by Yin et al. (2023).

In contrast, the reduction in sediment yield due to reforestation is smaller during the dry season and the effect of increased runoff becomes more apparent. The changes in vegetation types induced by the reforestation policy in the TGRA primarily enhance

runoff during the dry season. This finding is similar to that of Wang et al. (2019), who reported increased low flow during the dry season under the background of returning farmland to forests. The SWAT+ model simulations showed increases in canopy evaporation and transpiration by 21 mm/a during the dry season after the implementation of the GGP, with precipitation at 111 mm/a. Green water represents the rainfall that infiltrates the soil or is intercepted by vegetation and is subsequently returned to the atmosphere through evapotranspiration processes (Song et al., 2025). This increase in green water effectively enhances the precipitation to some extent, providing a localized supplement to rainfall. Xie et al. (2024) revealed that reforestation in China's croplands contributed to a precipitation increase of approximately 74.9 billion m^3/a. When cropland is converted to forests, the amount of vegetation transpiration or green water increases, promoting precipitation, which in turn enhances runoff during the dry season.

In summary, the GGP has distinct effects on sediment yield and water yield in the flood and dry seasons, although its influence on water yield is relatively limited compared to sediment yield. Wei et al. (2022) confirmed that under the scenario of cropland being converted to forests, variations in sediment yield are more prominent that those of water yield, particularly in high water years and the rainy season. During the flood season, reforestation in the TGRA mainly functions by reducing sediment loss. In contrast, during the dry season, it contributes more significantly to increasing runoff and regulating water resources. Therefore, the contribution of reforestation policies to hydrological processes in the TGRA is dynamic, and this aspect should be fully

considered in future management and planning.

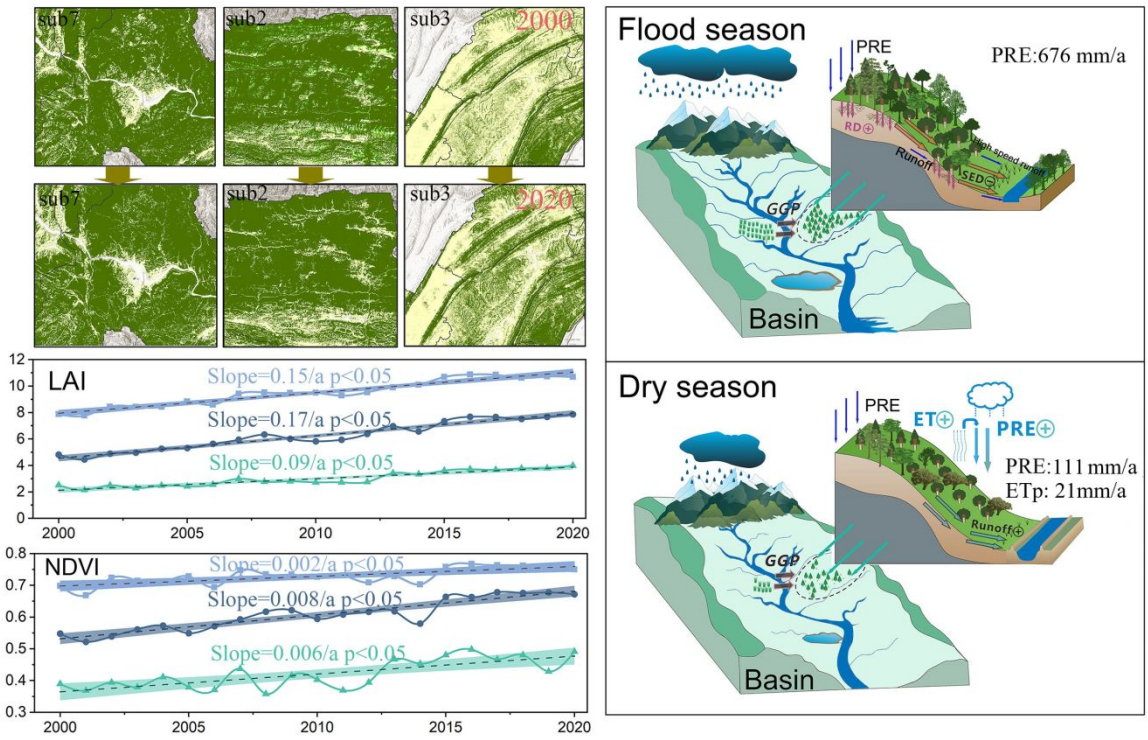

Fig. 10. Effects of the GPP on water yield and soil conservation during cropped hillslopes in different water periods (Wang et al., 2021). Notes: Green on the land use map indicates forests while yellow indicates cropland. On the right side, RD is the root depth, SED is sediment, and ET_P is plant transpiration. Three sub-basins with severe transformation from cropped hillslopes to forests from 2000 to 2020 are presented. Three lines of LAI and NDVI are displayed, with the top, middle bottom lines represent the flood, normal, and dry season, respectively.

4.3. Limitations and Future Works

This research has several limitations, which are listed as follows. First, the simulated value of low streamflow is not as accurate as that of high streamflow. Taking Yichang station as an example, the average measured runoff in the dry season was 20,000 m^3/s, while the simulated value was less than 10,000 m^3/s. Nevertheless, the simulation result is accurate for the flood and normal seasons, with high NS and R^2 values. It is noteworthy that this study aimed to analyze differences among scenarios and the same model parameters were applied under different scenarios. Therefore, the

model limitation on low streamflow values will not affect the comparative analysis.

Second, reforestation can not only influence water yield and sediment yields but also water quality and evapotranspiration. This study only discussed and analyzed two hydrology-related processes, not fully taking other processes into consideration. In the SWAT+ model, users can add land use management schedules to simulate the process of crop growth and pollutant transport. In future research, crop growth and pollutant transport processes can be simulated to fully capture differences in various factors under multiple scenarios.

Third, complex interactions exist between hydrological processes and vegetation processes. Although the SWAT+ model has high applicability in watershed-scale hydrological simulation, it simplifies real-world processes. The model cannot fully simulate some specific ecological processes, such as the complex interactions between vegetation dynamics, carbon and nitrogen cycles, and water cycles. The simulation of these processes is strongly affected by classification of land use data. In this study, the land use data classification used in the SWAT+ model was limited to broad categories such as cropland, forest, grassland, and shrubland. We assumed that the current level of land use detail is sufficient to meet the simulation accuracy required for the purpose of the study, and our calibration results also support this assumption. Nevertheless, refining the land use classification—such as by distinguishing between coniferous, deciduous, and broadleaf forests, or between rice and maize croplands—would allow for more accurate representation of vegetation-specific hydrological processes in future works.

5. Conclusions

The Three Gorges Reservoir Area is an important ecological protection zone in the Yangtze River Basin of China. This study utilized the SWAT+ model to simulate the water yield and sediment yield in the TGRA from 2000 to 2020 and assess the impacts of reforestation and climate change under various scenarios. Climatic factors were found to be the primary drivers of changes in water yield and sediment yield, with land use changes such as the reforestation policy also having a certain impact on runoff and a strong reducing effect on sediment yield. Moreover, the responses of water yield and sediment yield to the GGP exhibited seasonal characteristic. Reforestation had the most significant impact on increasing runoff during the dry season, while it mainly reduced sediment yield during the flood and normal seasons, especially in sub-basins in the eastern part of the TGRA. Based on the simulation results of past scenarios, we predicted runoff and soil retention from 2025 to 2050 under the SSP245 and SSP585 scenarios. Under the changing climate background, the predictions showed an upward trend of total runoff, and a downward trend of soil retention. To handle this situation, the local government can modify the direction of land use development and relevant ecological restoration policies. Thus, the simulation results under the three future land use development models can help provide references for policy adjustments. Furthermore, we suggest that in the future, the local government should consider ecological, and economic aspects as well as the well-being of residents, and effectively carry out reforestation to ensure the livelihoods of the residents. This study provides insights into the impact of the GGP and climate change on hydrological processes in

humid regions and offers guidance for future development pathways.

Reference

Arnold JG, Moriasi DN, Gassman PW, et al. (2012) SWAT: Model use, calibration, and validation. *Transactions of the ASABE* 55: 1491-1508.

Bai R, Wang X, Li J, et al. (2024) The impact of vegetation reconstruction on soil erosion in the Loess plateau. *Journal of Environmental Management* 363: 121382.

Bieger K, Arnold JG, Rathjens H, et al. (2019) Representing the Connectivity of Upland Areas to Floodplains and Streams in SWAT+. *JAWRA Journal of the American Water Resources Association* 55: 578-590.

Bieger K, Arnold JG, Rathjens H, et al. (2017) Introduction to SWAT+, a completely restructured version of the soil and water assessment tool. *JAWRA Journal of the American Water Resources Association* 53: 115-130.

Brighenti TM, Bonumá NB, Srinivasan R, et al. (2019) Simulating sub-daily hydrological process with SWAT: a review. *Hydrological Sciences Journal* 64: 1415-1423.

Bryan BA, Gao L, Ye Y, et al. (2018) China's response to a national land-system sustainability emergency. *Nature* 559: 193-204.

Bunel R, Copard Y, Caroline LB, et al. (2025) Impact of vegetation cover on hydro-sedimentary fluxes in the marly badlands of the Southern Alps (Draix-Bléone Critical Zone Observatory, SE France). *Geomorphology* 478: 109726.

Cai D, Ge Q, Wang X, et al. (2020) Contributions of ecological programs to vegetation restoration in arid and semiarid China. *Environmental Research Letters* 15: 114046.

Castellanos-Osorio G, López-Ballesteros A, Pérez-Sánchez J, et al. (2023) Disaggregated monthly SWAT+ model versus daily SWAT+ model for estimating environmental flows in Peninsular Spain. *Journal of Hydrology* 623: 129837.

Chen C, Gan R, Yang F, et al. (2022) Parameters optimization scheme and uncertainty analysis of runoff simulation based on SWAT model (In Chinese). *Yangtze River* 53.

Chen H, Fleskens L, Baartman J, et al. (2020) Impacts of land use change and climatic effects on streamflow in the Chinese Loess Plateau: A meta-analysis. *Science of the Total Environment* 703: 134989.

Chen X, Xu G, Zhang W, et al. (2019) Spatial variation pattern analysis of hydrologic processes and water quality in Three Gorges Reservoir Area. *Water* 11: 2608.

Cook BI, Mankin JS, Marvel K, et al. (2020) Twenty-First Century Drought Projections in the CMIP6 Forcing Scenarios. *John Wiley & Sons, Ltd*.

Daneshi A, Brouwer R, Najafinejad A, et al. (2021) Modelling the impacts of climate and land use change on water security in a semi-arid forested watershed using InVEST. *Journal of Hydrology* 593: 125621.

Derepasko D, Witing F, Peñas FJ, et al. (2023) Towards Adaptive Water Management—Optimizing River Water Diversion at the Basin Scale under Future Environmental Conditions. *Water*, 15.

Duda PB, Hummel PR, Donigian AS, et al. (2012) BASINS/HSPF: MODEL USE, CALIBRATION, AND VALIDATION. *Transactions of the ASABE* 55: 1523-1547.

Eekhout JP and Vente JD. (2020) How soil erosion model conceptualization affects soil loss projections

under climate change. *Progress in Physical Geography: Earth and Environment* 44: 212-232.
Francesconi W, Srinivasan R, Pérez-Miñana E, et al. (2016) Using the Soil and Water Assessment Tool (SWAT) to model ecosystem services: A systematic review. *Journal of Hydrology* 535: 625-636.
Gao G, Huang A, Ran L, et al. (2024) Dam regulation on extreme streamflow-sediment relationships along the Yangtze River Basin. *Science Bulletin*.
Gao Jixi ZHZWCXSWXTZYSHIY. (2024) China regional 250m normalized difference vegetation index data set (2000-2023). In: National Tibetan Plateau Data C (ed). National Tibetan Plateau Data Center.
Gebre AM, Belete MD and Belayneh MZ. (2024) Soil Loss and Sediment Yield Prediction in Lake Hawassa Sub-Basin, Central Rift Valley Basin, Ethiopia. *Air, Soil and Water Research* 17.
Hagemann S, Chen C, Clark DB, et al. (2013) Climate change impact on available water resources obtained using multiple global climate and hydrology models. *Earth System Dynamics* 4: 129-144.
Hattermann FF, Huang S and Koch H. (2015) Climate change impacts on hydrology and water resources.
Huang C, Zhao D and Deng L. (2022) Landscape pattern simulation for ecosystem service value regulation of Three Gorges Reservoir Area, China. *Environmental Impact Assessment Review* 95: 106798.
Huang C, Zhao D, Liao Q, et al. (2023) Linking landscape dynamics to the relationship between water purification and soil retention. *Ecosystem Services* 59: 101498.
Janjić J and Tadić L. (2023) Fields of application of SWAT hydrological model—a review. *Earth* 4: 331-344.
Jian S, Zhao C, Fang S, et al. (2015) Effects of different vegetation restoration on soil water storage and water balance in the Chinese Loess Plateau. *Agricultural and Forest Meteorology* 206: 85-96.
Leone M, Gentile F, Lo Porto A, et al. (2024) Setting an environmental flow regime under climate change in a data-limited Mediterranean basin with temporary river. *JOURNAL OF HYDROLOGY-REGIONAL STUDIES* 52.
Lewis SL, Wheeler CE, Mitchard ET, et al. (2019) Restoring natural forests is the best way to remove atmospheric carbon. Nature Publishing Group.
Li BY and Wang YC. (2024) Impact of the Grain-for-Green Programme and climate change on the soil erosion decline in the Yangtze River, China. *JOURNAL OF GEOGRAPHICAL SCIENCES* 34: 527-542.
Li M, Di ZH and Duan QY. (2021) Effect of sensitivity analysis on parameter optimization: Case study based on streamflow simulations using the SWAT model in China. *Journal of Hydrology* 603.
Li Z, Deng X, Wu F, et al. (2015) Scenario analysis for water resources in response to land use change in the middle and upper reaches of the Heihe River Basin. *Sustainability* 7: 3086-3108.
Liang X, Guan Q, Clarke KC, et al. (2021) Understanding the drivers of sustainable land expansion using a patch-generating land use simulation (PLUS) model: A case study in Wuhan, China. *Computers, Environment and Urban Systems* 85: 101569.
Liang X, Lettenmaier DP and Wood EF. (1996) One-dimensional statistical dynamic representation of subgrid spatial variability of precipitation in the two-layer variable infiltration capacity model. *Journal of Geophysical Research-Atmospheres* 101: 21403-21422.
Liu R, Wang J, Shi J, et al. (2014) Runoff characteristics and nutrient loss mechanism from plain farmland under simulated rainfall conditions. *Science of the Total Environment* 468-469: 1069-

1077.

Liu ZF, Xu ZX, Huang JX, et al. (2010) Impacts of climate change on hydrological processes in the headwater catchment of the Tarim River basin, China. *HYDROLOGICAL PROCESSES* 24: 196-208.

Lowe SA. (2010) Sanitary Sewer Design Using EPA Storm Water Management Model (SWMM). *Computer Applications in Engineering Education* 18: 203-212.

Luo Y, Wang H, Meersmans J, et al. (2021) Modeling soil erosion between 1985 and 2014 in three watersheds on the carbonate-rock dominated Guizhou Plateau, SW China, using WaTEM/SEDEM. *Progress in Physical Geography: Earth and Environment* 45: 53-81.

McFarlane D, Stone R, Martens S, et al. (2012) Climate change impacts on water yields and demands in south-western Australia. *Journal of Hydrology* 475: 488-498.

Molina A, Vanacker V, Balthazar V, et al. (2012) Complex land cover change, water and sediment yield in a degraded Andean environment. *Journal of Hydrology* 472: 25-35.

Nash JE and Sutcliffe JV. (1970) River flow forecasting through conceptual models part I—A discussion of principles. *Journal of Hydrology* 10: 282-290.

Nepal D, Parajuli PB, Ouyang Y, et al. (2023) Assessing hydrological and water quality responses to dynamic landuse change at watershed scale in Mississippi. *Journal of Hydrology* 625: 129983.

NFGA. (2020) Twenty Years of Returning Farmland to Forests and Grasslands in China (1999-2019). National Forestry and Grassland Administration.

Nkwasa A, Chawanda CJ, Msigwa A, et al. (2020) How Can We Represent Seasonal Land Use Dynamics in SWAT and SWAT+ Models for African Cultivated Catchments? *Water*, 12.

Noori N and Kalin L. (2016) Coupling SWAT and ANN models for enhanced daily streamflow prediction. *Journal of Hydrology* 533: 141-151.

Qin PC, Xu HM, Liu M, et al. (2020) Climate change impacts on Three Gorges Reservoir impoundment and hydropower generation. *Journal of Hydrology* 580.

Rockström J, Mazzucato M, Andersen LS, et al. (2023) Why we need a new economics of water as a common good. *Nature* 615: 794-797.

Shi P, Chen C, Srinivasan R, et al. (2011) Evaluating the SWAT model for hydrological modeling in the Xixian watershed and a comparison with the XAJ model. *Water resources management* 25: 2595-2612.

Sidle RC, Gomi T, Usuga JCL, et al. (2017) Hydrogeomorphic processes and scaling issues in the continuum from soil pedons to catchments. *Earth-Science Reviews* 175: 75-96.

Song ZH, Zhang XQ, Xu JJ, et al. (2025) Vegetation greening promotes the conversion of blue water to green water by enhancing transpiration. *Journal of Hydrology* 658.

Sun G, Zhou G, Zhang Z, et al. (2006) Potential water yield reduction due to forestation across China. *Journal of Hydrology* 328: 548-558.

Sun W, Shao Q, Liu J, et al. (2014) Assessing the effects of land use and topography on soil erosion on the Loess Plateau in China. *Catena* 121: 151-163.

Taylor KE. (2001) Summarizing multiple aspects of model performance in a single diagram. *Journal of Geophysical Research-Atmospheres* 106: 7183-7192.

Thrasher B, Wang W, Michaelis A, et al. (2022) NASA global daily downscaled projections, CMIP6. *Scientific data* 9: 262.

Tianjiao F, Tianxing W, Keesstra SD, et al. (2023) Long-term effects of vegetation restoration on hydrological regulation functions and the implications to afforestation on the Loess Plateau.

Agricultural and Forest Meteorology 330: 109313.

Uniyal B, Kosatica E and Koellner T. (2023) Spatial and temporal variability of climate change impacts on ecosystem services in small agricultural catchments using the Soil and Water Assessment Tool (SWAT). *Science of The Total Environment* 875.

Wallington K and Cai X. (2023) Updating SWAT+ to Clarify Understanding of In-Stream Phosphorus Retention and Remobilization: SWAT+P.R&R. *Water Resources Research* 59: e2022WR033283.

Wang g, Xia j, Li x, et al. (2021) Critical advances in understanding ecohydrological processes of terrestrial vegetation: From leaf to watershed scale (in Chinese). *Chinese Science Bulletin* 66: 3667-3683.

Wang H and Sun F. (2021) Variability of annual sediment load and runoff in the Yellow River for the last 100 years (1919–2018). *Science of the Total Environment* 758: 143715.

Wang S, Fu BJ and Liang W. (2016) Developing policy for the Yellow River sediment sustainable control. *NATIONAL SCIENCE REVIEW* 3: 162-164.

Wang W, Chen L, Zhu Y, et al. (2019) Is returning farmland to forest an effective measure to reduce phosphorus delivery across distinct spatial scales? *Journal of Environmental Management* 252: 109663.

Wang Y, Liu X, Li J, et al. (2022) Quantifying the spatial flow of soil conservation service to optimize land-use pattern under ecological protection scenarios. *Frontiers in Earth Science* 10: 957520.

Wang Z, Fu B, Wu X, et al. (2023) Vegetation resilience does not increase consistently with greening in China's Loess Plateau. *Communications Earth & Environment* 4: 336.

Wei C, Dong XH, Yu D, et al. (2022) An alternative to the Grain for Green Program for soil and water conservation in the upper Huaihe River basin, China. *JOURNAL OF HYDROLOGY-REGIONAL STUDIES* 43.

Wu J and Gao XJ. (2013) A gridded daily observation dataset over China region and comparison with the other datasets (in Chinese). *Chinese Journal of Geophysics Chinese Edition* 56: 1102-1111.

Wu Q, Ke L, Wang J, et al. (2023) Satellites reveal hotspots of global river extent change. *Nature Communications* 14: 1587.

Xie D, Zhang Y, Zhang M, et al. (2024) Hydrological impacts of vegetation cover change in China through terrestrial moisture recycling. *Science of the Total Environment* 915: 170015.

Xiong L, Xu X, Ren D, et al. (2019) Enhancing the capability of hydrological models to simulate the regional agro-hydrological processes in watersheds with shallow groundwater: Based on the SWAT framework. *Journal of Hydrology* 572: 1-16.

Xu H, Taylor RG and Xu Y. (2011) Quantifying uncertainty in the impacts of climate change on river discharge in sub-catchments of the Yangtze and Yellow River Basins, China. *Hydrol. Earth Syst. Sci.* 15: 333-344.

Xu XB, Yang GS, Tan Y, et al. (2020) Unravelling the effects of large-scale ecological programs on ecological rehabilitation of China's Three Gorges Dam. *Journal of Cleaner Production* 256.

Yifru BA, Chung I-M, Kim M-G, et al. (2021) Assessing the Effect of Land/Use Land Cover and Climate Change on Water Yield and Groundwater Recharge in East African Rift Valley using Integrated Model. *Journal of Hydrology: Regional Studies* 37: 100926.

Yin S, Gao G, Ran L, et al. (2023) Extreme streamflow and sediment load changes in the Yellow River Basin: Impacts of climate change and human activities. *Journal of Hydrology* 619: 129372.

Zhang L, Wang J, Bai Z, et al. (2015) Effects of vegetation on runoff and soil erosion on reclaimed land

in an opencast coal-mine dump in a loess area. *Catena* 128: 44-53.

Zhang Y, Zhong P-a, Chen J, et al. (2017) Impacts of Climate Change and Human Activities on the Three Gorges Reservoir Inflow. *Water*, 9.

Zhao J, Cheng H, Cao J, et al. (2023) Orchestrated decline of Asian summer monsoon and Atlantic meridional overturning circulation in global warming period. *The Innovation Geoscience* 100011.

Zhou J, Liu Q, Liang L, et al. (2024a) Water constraints enhanced by revegetation while alleviated by increased precipitation on China's water-dominated Loess Plateau. *Journal of Hydrology* 640: 131731.

Zhou Y, Huang Q, Wu P, et al. (2024b) Seasonal variations in ecosystem service supply and demand based on the SWAT model: A case study in the Guanting Reservoir Basin, China. *Ecological Indicators* 158: 111552.

Zhou ZC, Gan ZT, Shangguan ZP, et al. (2009) China's Grain for Green Program has reduced soil erosion in the upper reaches of the Yangtze River and the middle reaches of the Yellow River. *INTERNATIONAL JOURNAL OF SUSTAINABLE DEVELOPMENT AND WORLD ECOLOGY* 16: 234-239.

Zhu G, Deng L and Shangguan Z. (2018) Effects of soil aggregate stability on soil N following land use changes under erodible environment. *Agriculture, Ecosystems & Environment* 262: 18-28.

Zhu H, Jiang Z and Li L. (2021) Projection of climate extremes in China, an incremental exercise from CMIP5 to CMIP6. *Science Bulletin* 66: 2528-2537.

Supplement of

Runoff and sediment dynamics induced by the "Grain for Green" programme: a case study in the Three Gorges Reservoir Area, China

Text S1.

The Patch-generating Land Use Simulation (PLUS) model, enhances the spatial-temporal dynamics and prediction of land use changes by integrating spatial factors with geographic cell dynamics. It combines existing transformation and pattern analysis strategies and introduces the Land Expansion Analysis Strategy (LEAS), which avoids exponential growth in transformation types while retaining the ability to analyze land use changes. LEAS method employs a random forest algorithm to assess land use expansion and driving factors, predicting land use development probabilities. The PLUS model also includes a unique CA model based on random patch seeds, incorporating both "top-down" and "bottom-up" mechanisms to simulate dynamic land use changes. The combination of PLUS and the multi-objective optimization algorithm can enhance the robustness of the model (Li et al., 2022). For more details on the model, see the work of Liang et al. (2021).

The Kappa coefficient is integrated into the PLUS model, are used to assess the accuracy of simulation results. It effectively reflects the degree of consistency between the simulated outputs and actual observations. Generally, a Kappa value greater than 0.8 indicates that the simulation results are highly reliable. The Kappa coefficient is calculated using the following formula:

$$Kappa = \frac{K_1 - K_2}{1 - K_2} \quad (1)$$

where K_1 is the observed agreement (equivalent to the overall accuracy), and K_2 is the expected agreement by chance, computed from the marginal probabilities of each class in the confusion matrix.

LEAS was used to identify the driving factors and spatial distribution patterns of land use changes. The scientific selection of driving factors is essential for accurate land cover simulation. Considering that land cover change is influenced by a combination of topographic, environmental, and socioeconomic factors, twelve driving factors were selected in this study based on data availability, spatial heterogeneity, and inter-factor correlation. The selection was informed by previous study and the characteristics of the study area. These factors include elevation, slope, precipitation (2020 year), and temperature (2020 year) to represent natural environmental conditions; GDP (2020) and population density (2020) to capture socioeconomic influences; and Euclidean distances to major roads, secondary roads, tertiary roads, county centers, railways, and water bodies to reflect spatial accessibility. All distance variables were calculated using the Euclidean distance tool in GIS, and road network data were obtained from OpenStreetMap (Fig.S1).

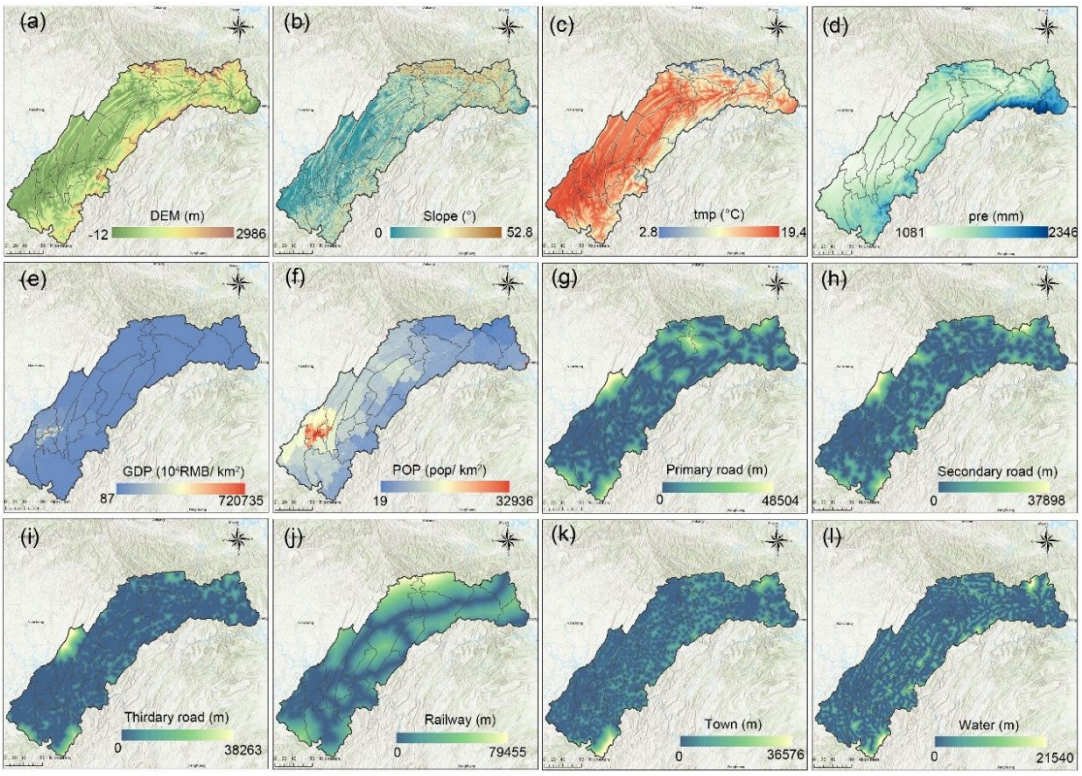

Fig. S1. Drivers of the PLUS model

Table S1. Future land use scenario area transfer matrix (%)

Pattern	Types	Shrubland	Grassland	Cultivated land	Waterbody	Built-up land	Unused land	Forests
Ecological pattern	Shrubland	94.45	0.15	0.35	0	0	0	5.05
	Grassland	5	94.68	0.32	0	0	0	0
	Cultivated land	0.5	0.05	96.95	0	0	0	2.5
	Waterbody	0	0	0	98	0	2	0
	Built-up land	0	0	0	0	100	0	0
	Unused land	1.69	0.01	2	5	45	44.17	2.13
	Forests	0.21	1.03	0.72	0	0	0	98.04
Eco-economy pattern	Shrubland	98.49	0.15	0.35	0	0.8	0.14	0.07
	Grassland	0	99.64	0.32	0	0	0.04	0
	Cultivated land	0	0	98.88	0	0.5	0.62	0
	Waterbody	0	0	0	100	0	0	0
	Built-up land	0	0	0	0	100	0	0
	Unused land	0	0	0	0	70	30	0
	Forests	0.21	1.03	0.72	0	2.6	0.88	94.56
Economy pattern	Shrubland	93.95	0.15	0.35	0	0.5	0	5.05
	Grassland	5	94.68	0.32	0	0	0	0
	Cultivated land	0.5	0.05	96.45	0	0.5	0	2.5
	Waterbody	0	0	0	98	0	2	0
	Built-up land	0	0	0	0	100	0	0
	Unused land	1.69	0.01	2	5	65	24.17	2.13
	Forests	0.21	1.03	0.72	0	1.7	0	96.34

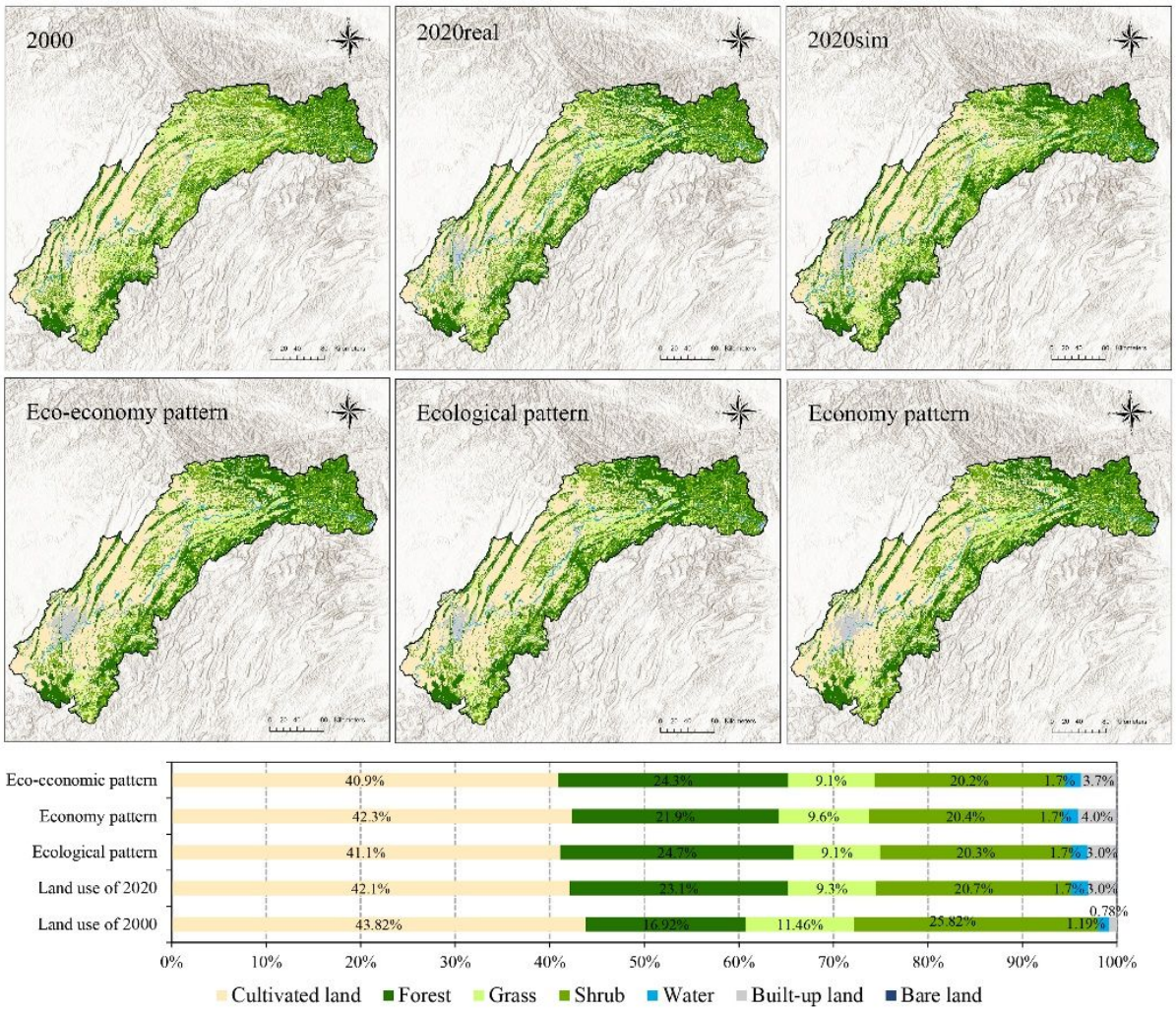

Fig. S2. Land use in 2000, 2020, simulated land use of 2020 and the projected land use map in 2035 simulated by the PLUS model

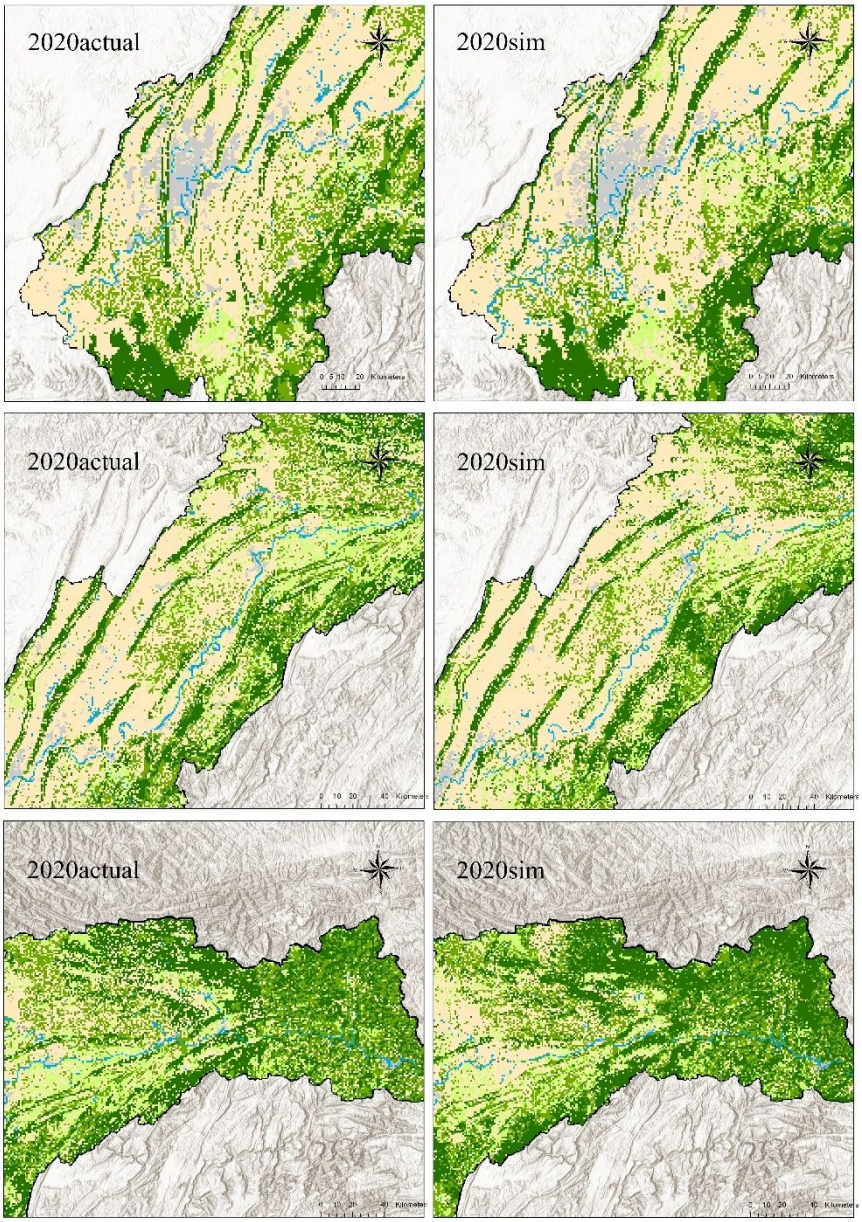

Fig. S3. The figure details of simulated land use and actual land use in 2020.

Table S2. 14 CMIP6 modes and selection scenarios used in this study

Number	GCMS	Historical	SSP245	SSP585
1	ACCESS-ESM1-5	√	√	√
2	BCC-ESM1	√	√	√
3	HadGEM3-GC31-LL	√	√	√
4	INM-CM4-8	√	√	√
5	INM-CM5-0	√	√	√
6	IPSL-CM6A-LR	√	√	√
7	GFDL-CM4	√	√	√
8	NorESM2-LM	√	√	√
9	CNRM-ESM2-1	√	√	√
10	CNRM-CM6-1	√	√	√
11	MPI-ESM1-2-HR	√	√	√
12	MRI-ESM2-0	√	√	√
13	IPSL-CM6A-LR	√	√	√
14	MIROC6	√	√	√

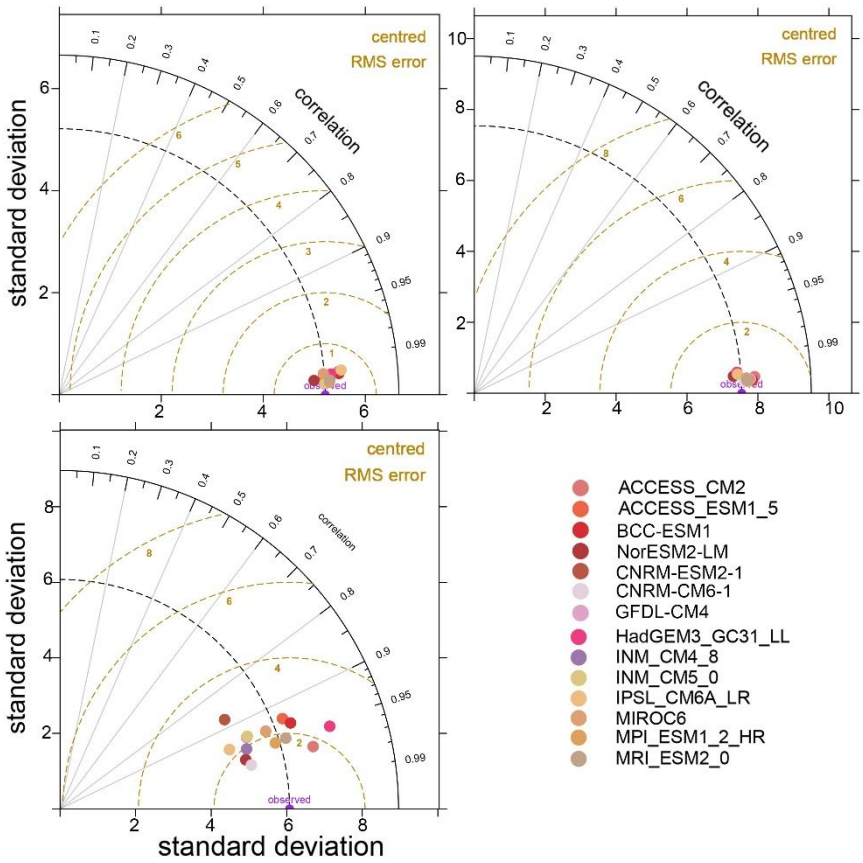

Fig. S4. Taylor chart evaluation for different GCMS. (a) Tmax, (b) Tmin, (c) PRE

Table S3. Comparison of simulation results before and after calibration

Variables		Before calibration		After calibration	
	Station	NS	|PBIAS|	NS	|PBIAS|
Flow_out (m^3/s)	Yichang	0.75	29.1	0.84	12.02
	Beibei	0.87	24	0.89	3.01
	Cuntan	0.72	32.7	0.82	16.4
	Wanxian	0.70	32.7	0.80	16.4
Sediment (tons)	Yichang	0.45	34.1	0.54	20.5

Table S4. Comparison of runoff simulation results with SWAT model

		SWAT			SWAT+		
Period	Station	R^2	NS	|PBIAS|	R^2	NS	|PBIAS|
Calibration	Yichang	0.87	0.78	17.3	0.94	0.84	12.02
	Beibei	0.77	0.74	13.4	0.92	0.89	3.01
	Cuntan	0.87	0.73	19.7	0.94	0.82	16.4
	Wanxian	0.82	0.72	15.5	0.93	0.80	16.4
Validation	Yichang	0.80	0.64	17.4	0.87	0.67	12.1
	Beibei	0.74	0.71	12.6	0.92	0.88	-0.89
	Cuntan	0.83	0.63	18.8	0.93	0.74	9.75
	Wanxian	0.77	0.61	22.2	0.89	0.74	15.27

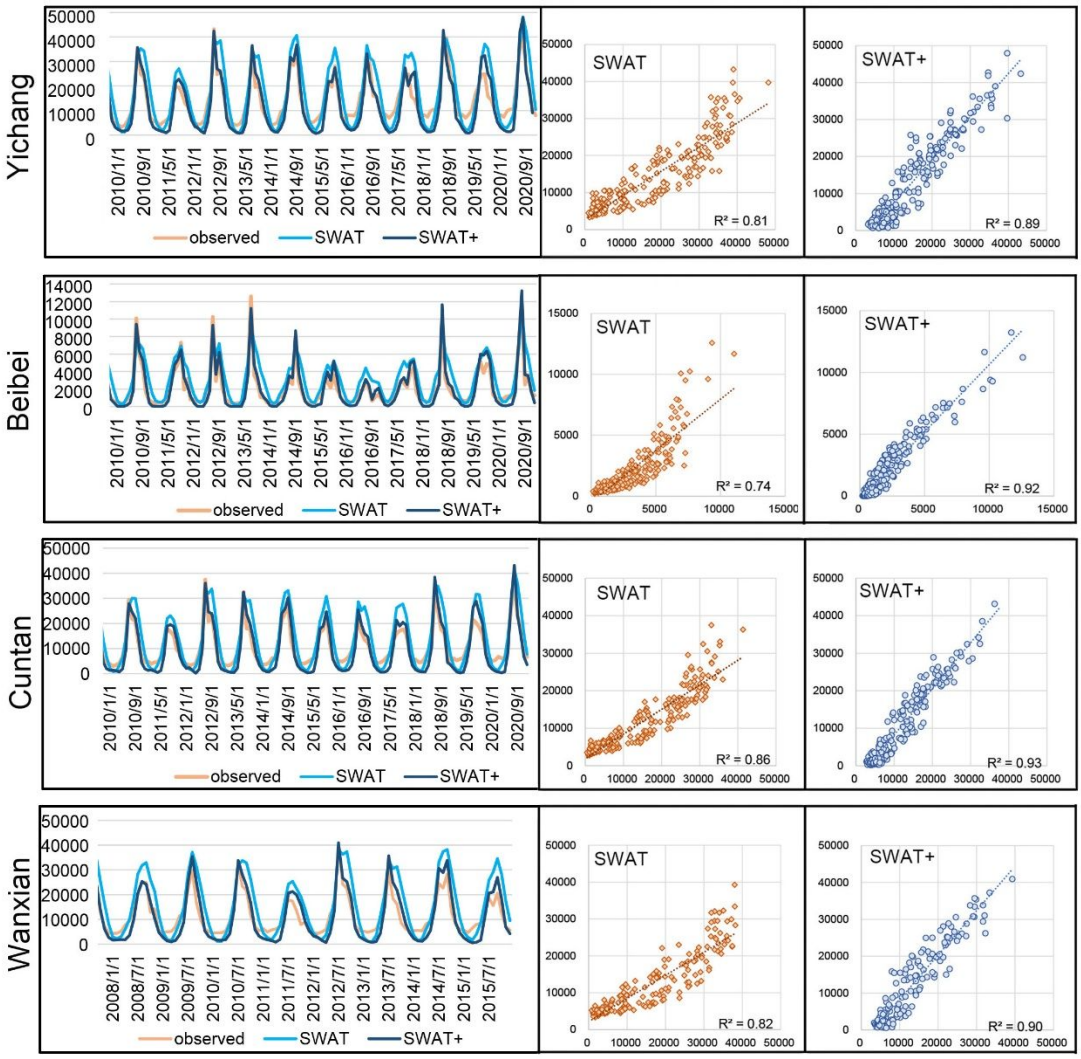

Fig. S5. Comparison of SWAT and SWAT+ runoff simulation results at four hydrological stations (The line chart only shows the simulation results during the validation period).

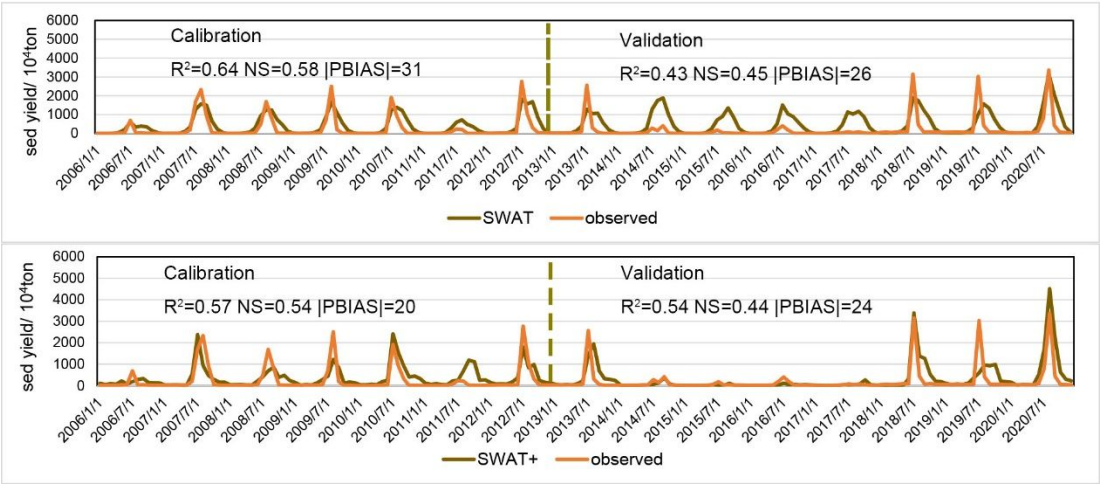

Fig. S6. Calibration and validation comparison of sediment simulation results from 2006-2020

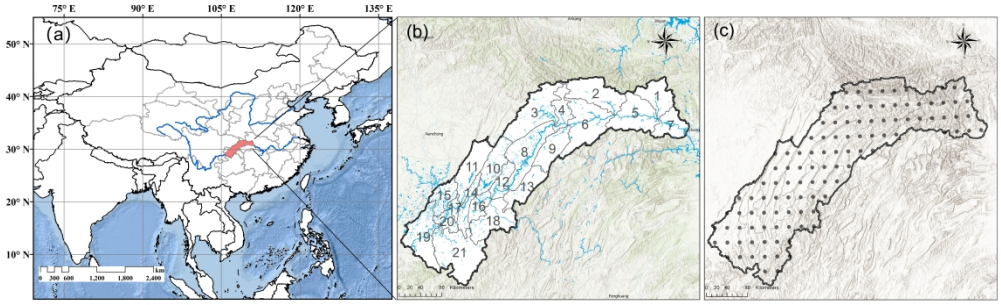

626x191mm (300 x 300 DPI)

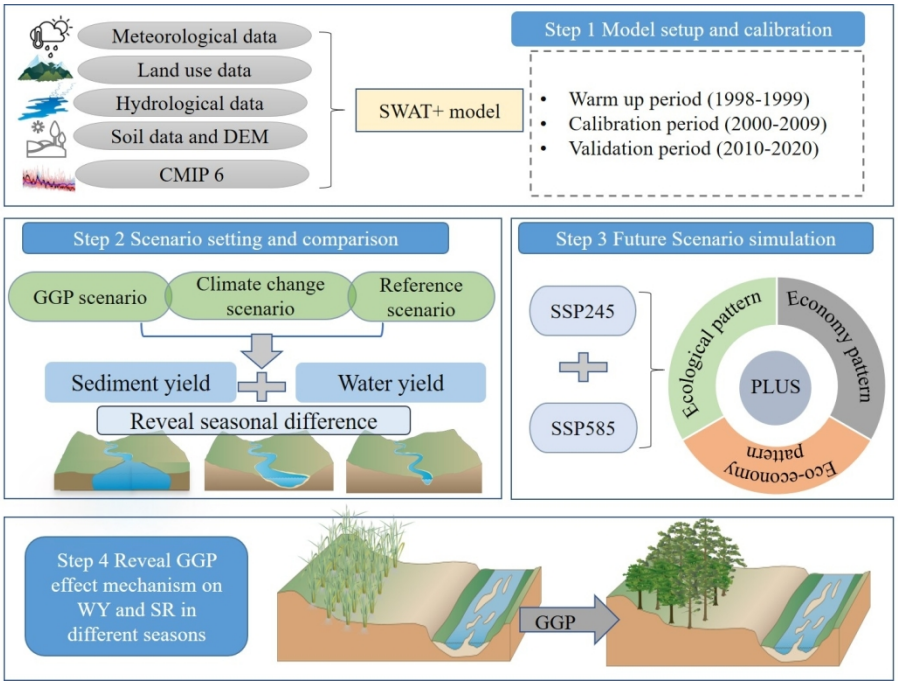

274x186mm (150 x 150 DPI)

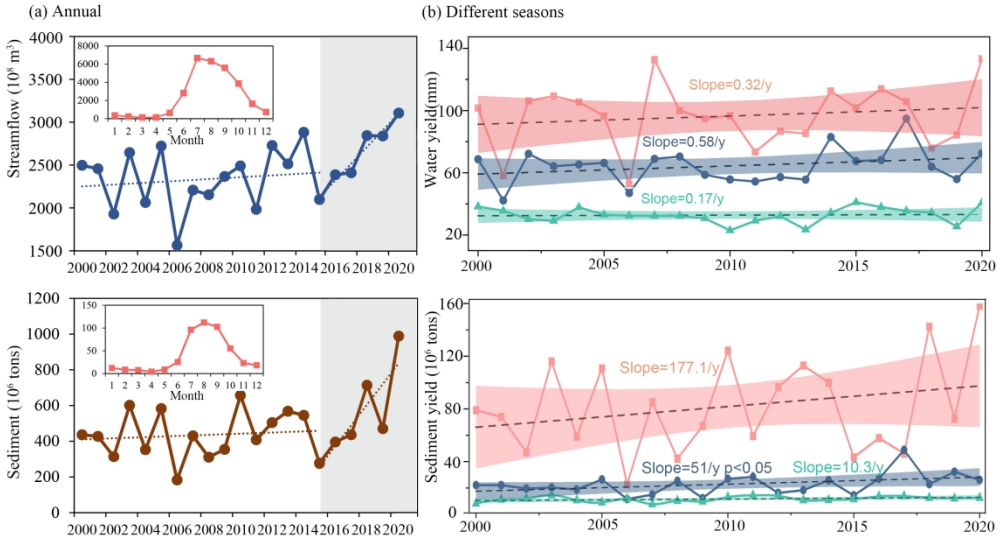

249x139mm (300 x 300 DPI)

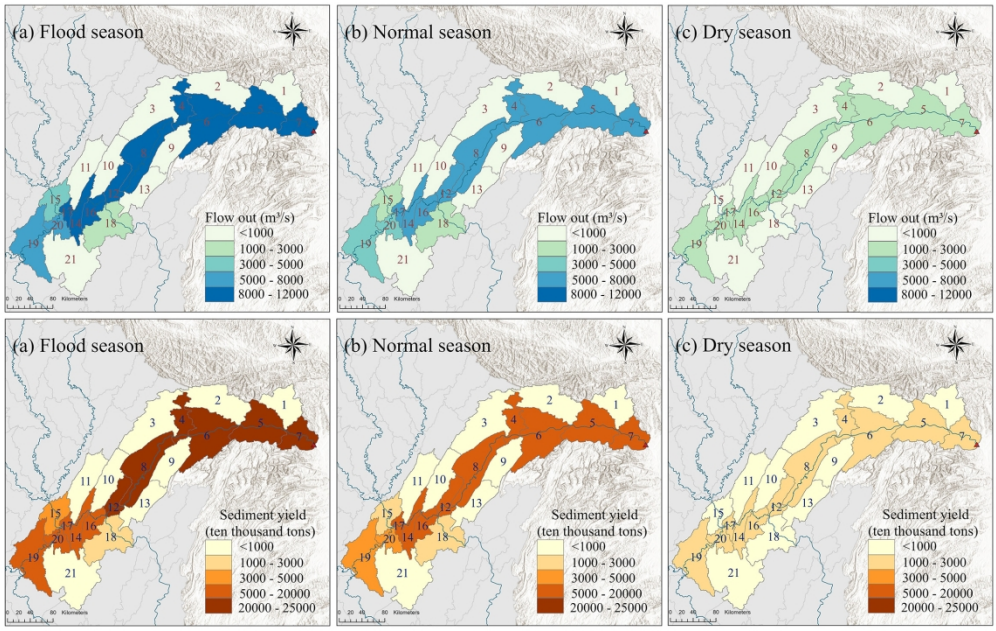

199x125mm (300 x 300 DPI)

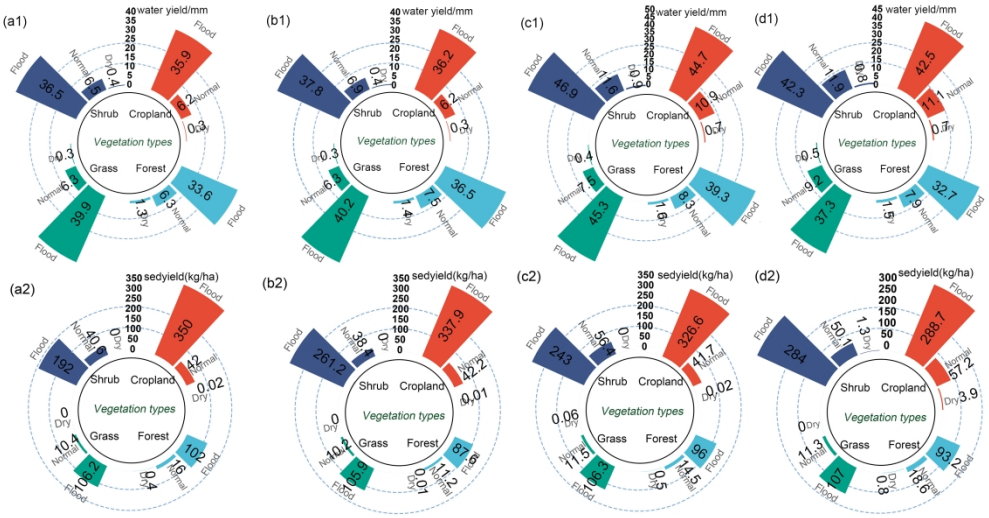

299x159mm (300 x 300 DPI)

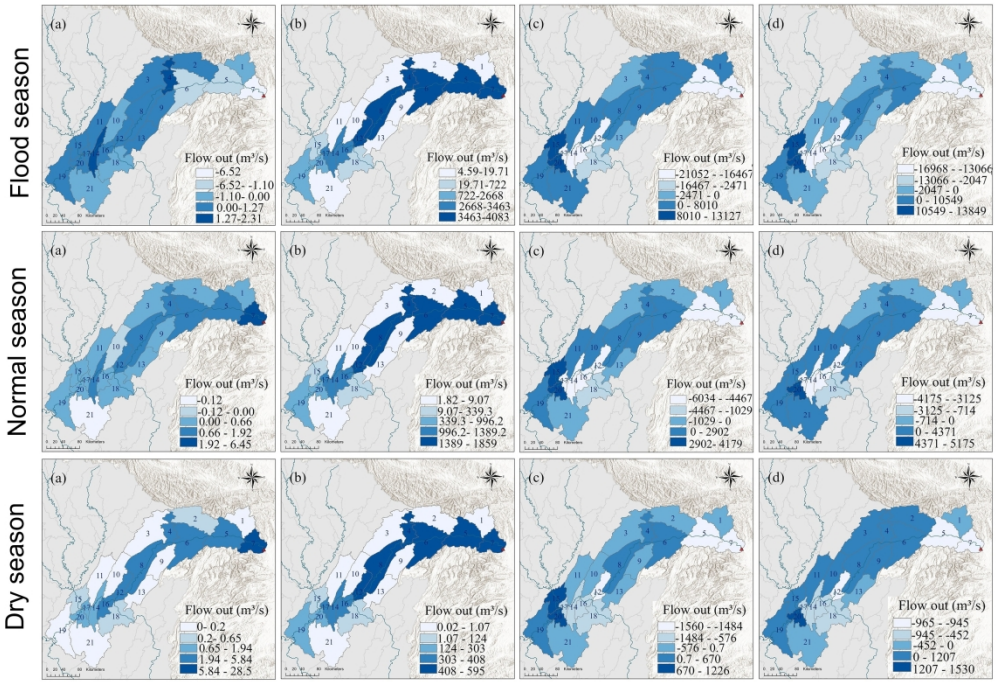

312x215mm (300 x 300 DPI)

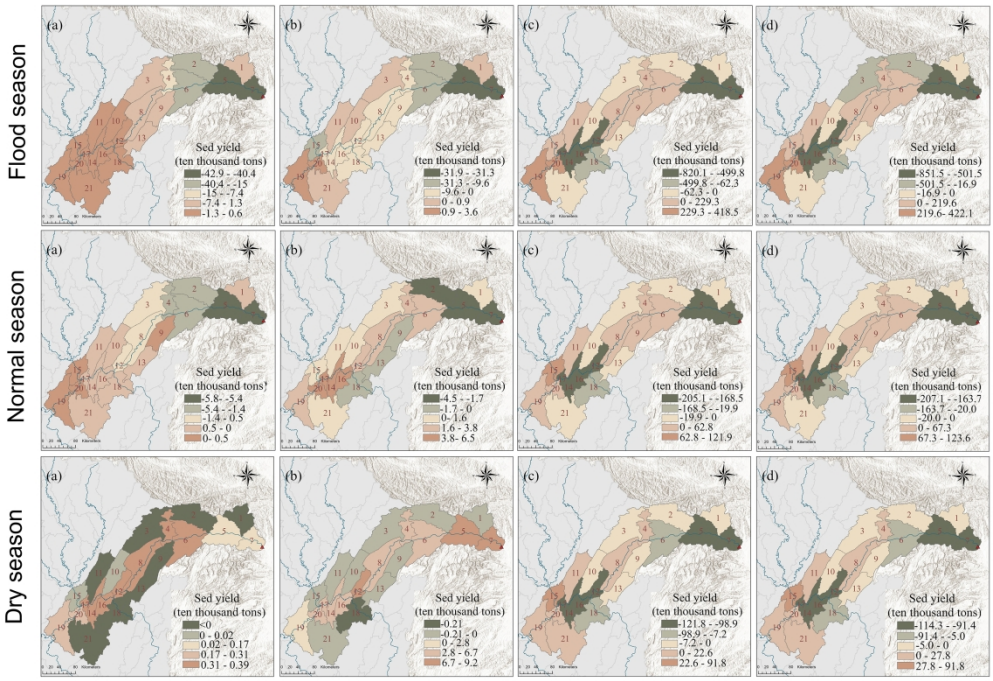

299x205mm (300 x 300 DPI)

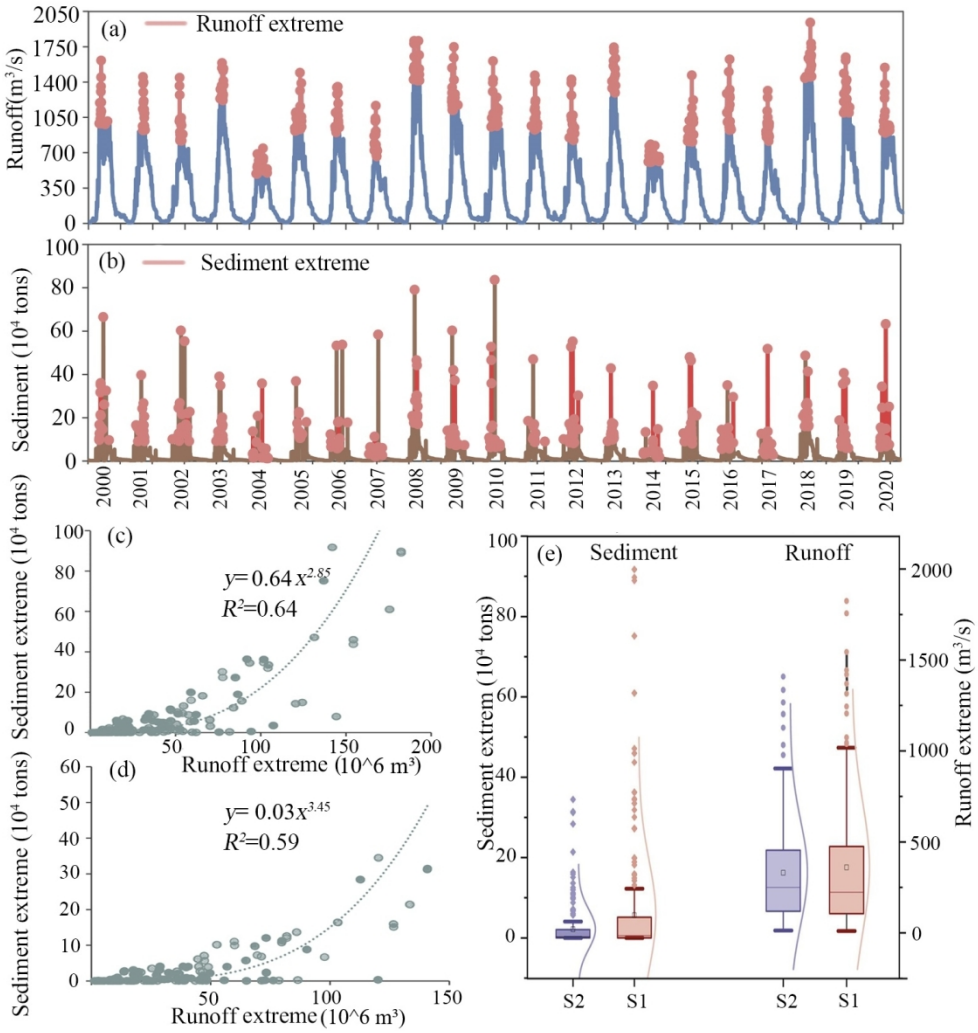

135x143mm (300 x 300 DPI)

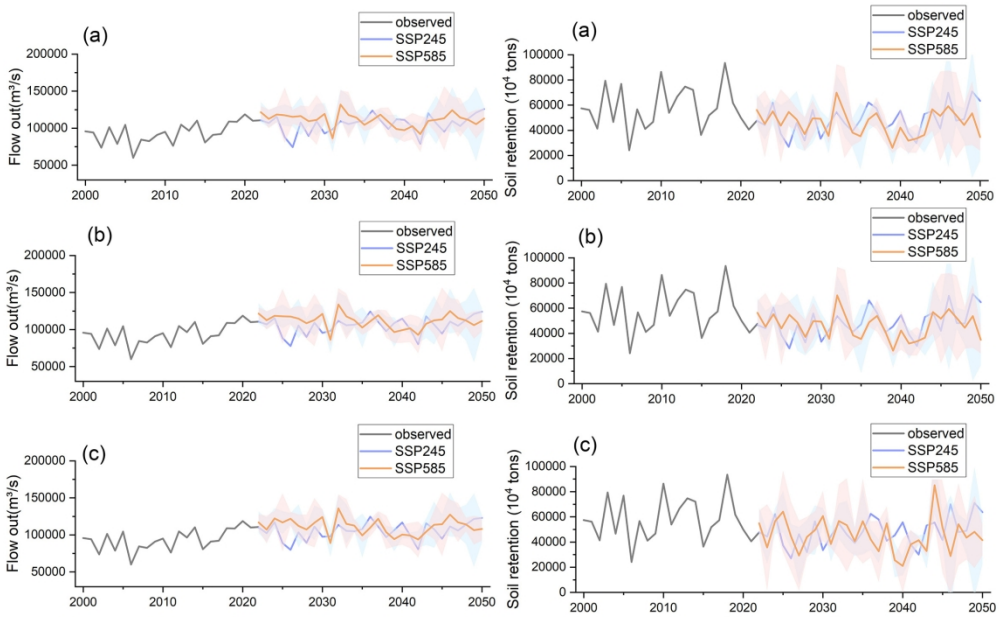

Compared to 2000-2023	SSP245 Water yield	SSP585 Water yield	SSP245 Soil retention	SSP585 Soil retention
(a) Eco	Increase by 12.96%	Increase by 19.17%	Decrease by 18.11%	Decrease by 22.52%
(b) Eco-economy	Increase by 13.08%	Increase by 19.29%	Decrease by 17.85%	Decrease by 22.20%
(c) Economy	Increase by 13.16%	Increase by 19.30%	Decrease by 18.40%	Decrease by 22.63%

199x157mm (300 x 300 DPI)

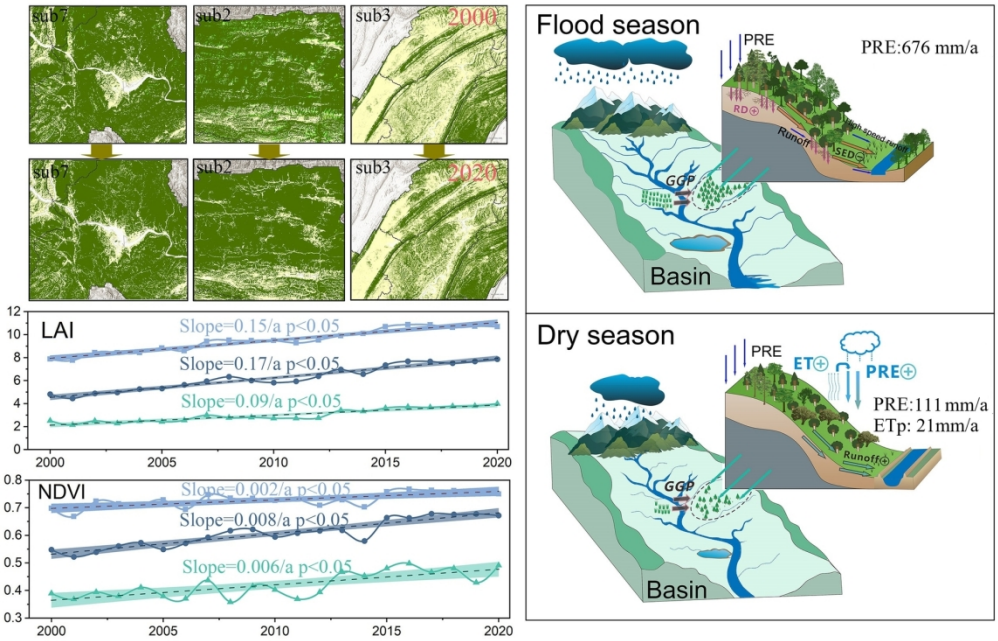

80x51mm (600 x 600 DPI)

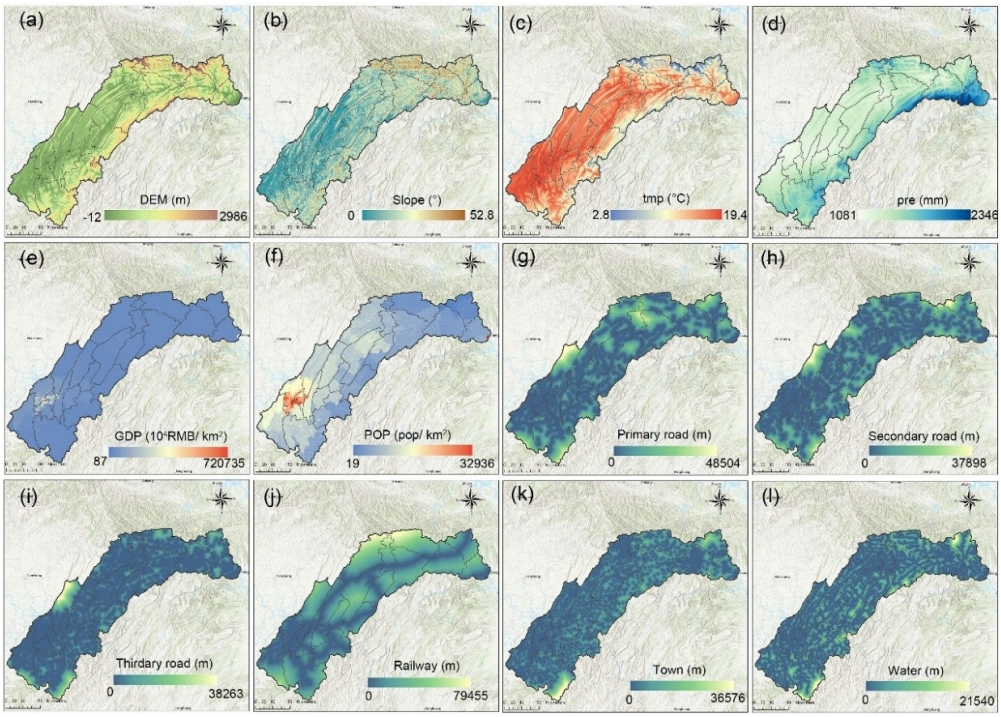

142x101mm (220 x 220 DPI)

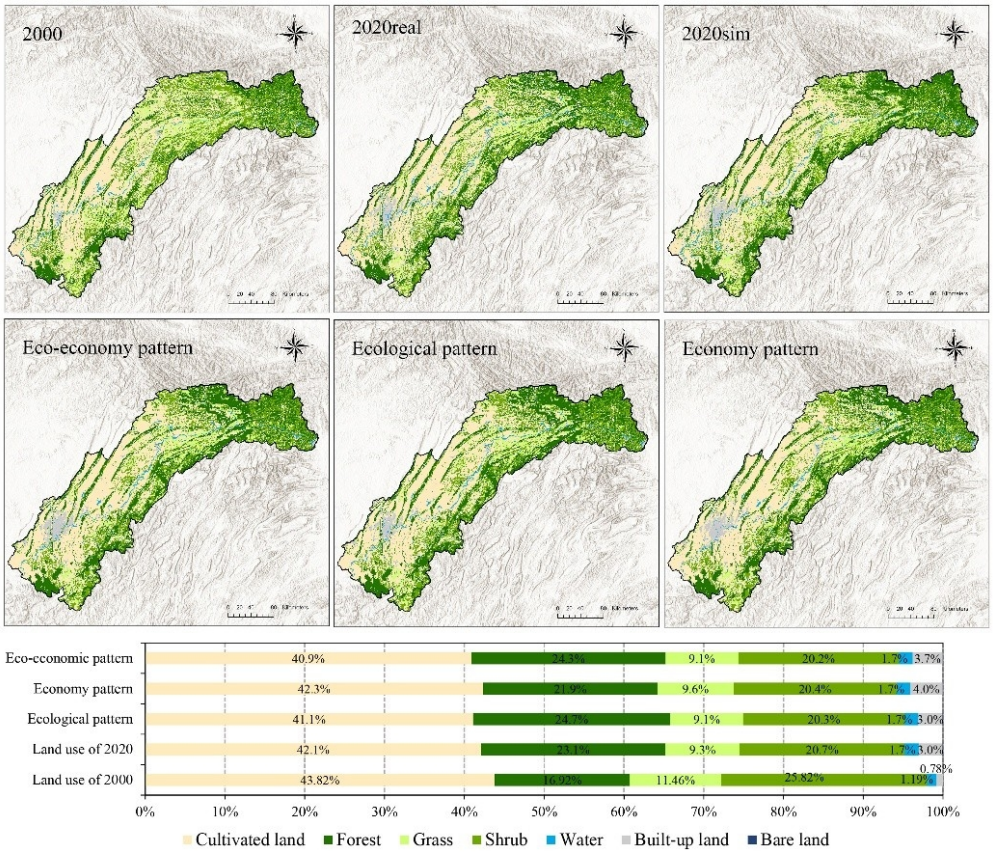

119x102mm (220 x 220 DPI)

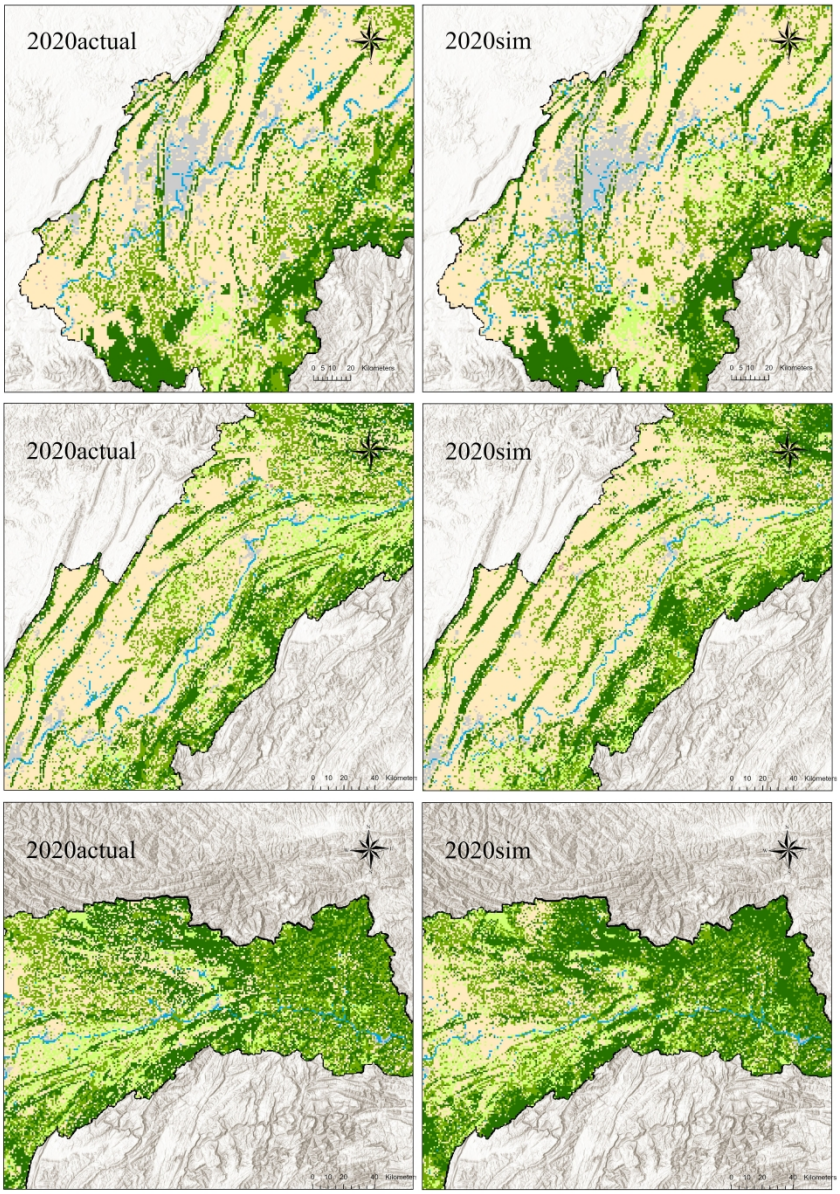

426x607mm (300 x 300 DPI)

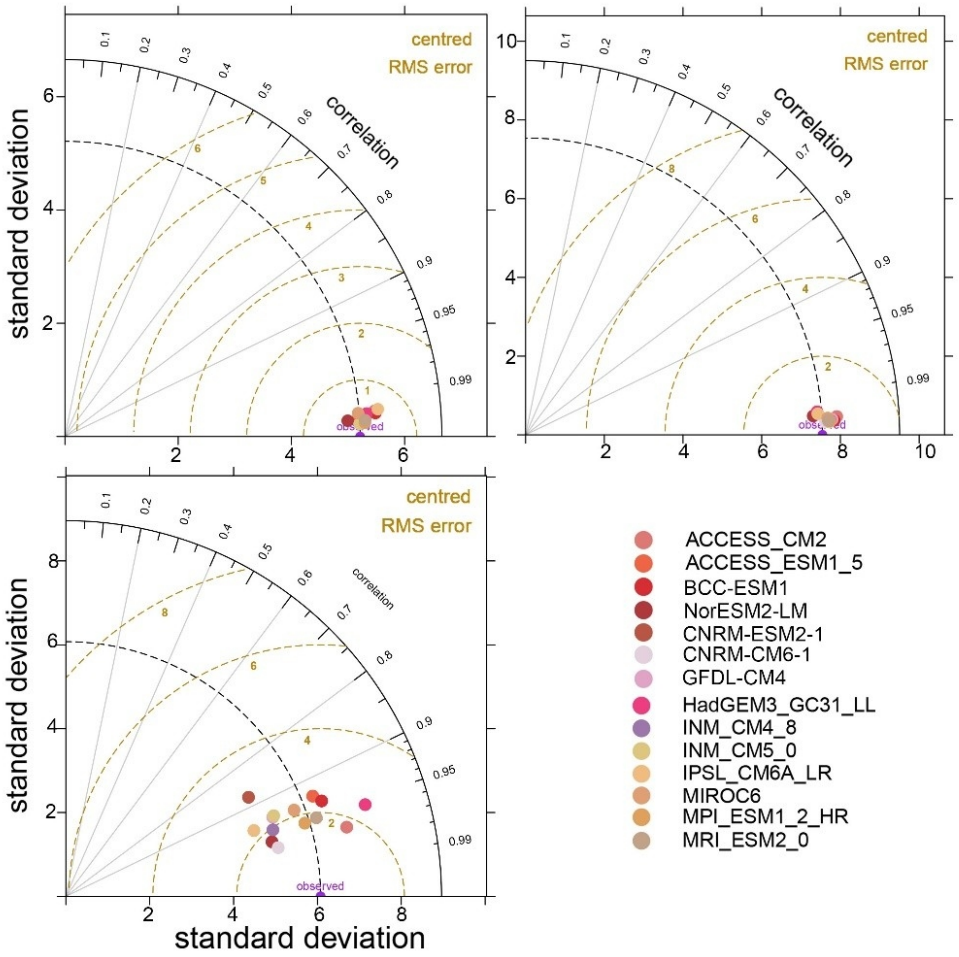

118x114mm (220 x 220 DPI)

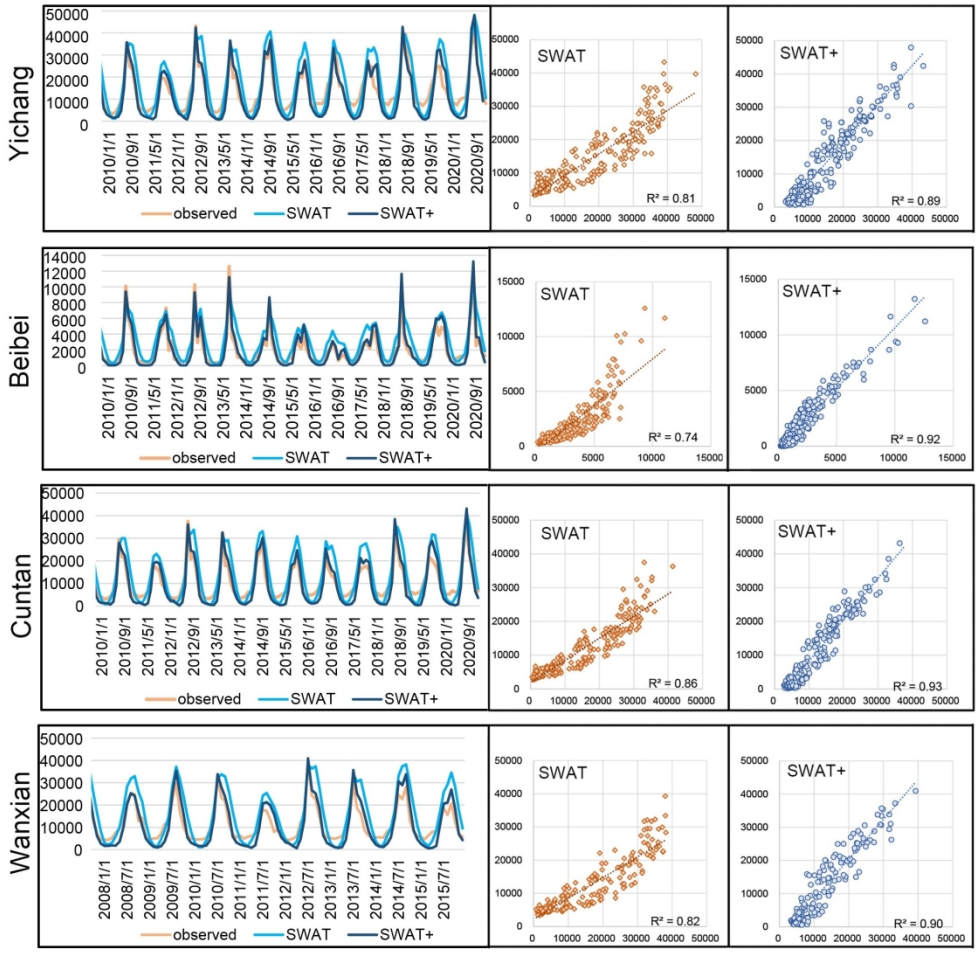

186x182mm (300 x 300 DPI)

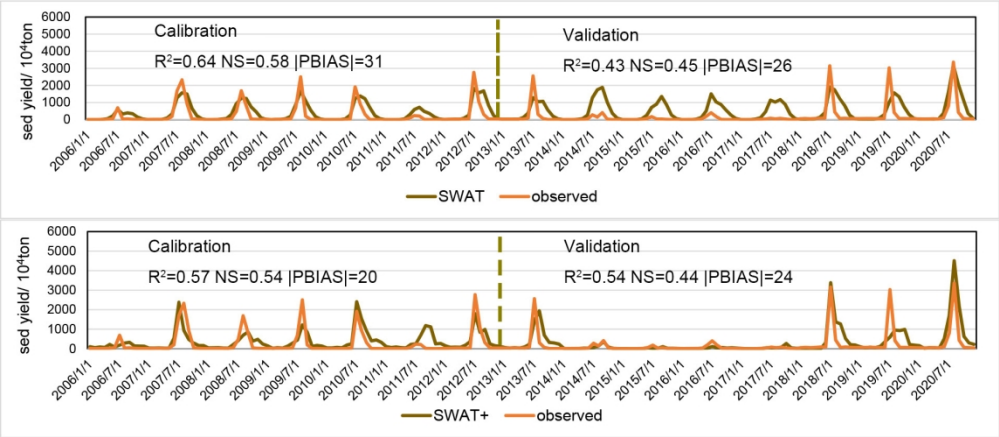

162x72mm (300 x 300 DPI)